# Carfilzomib Treatment Causes Molecular and Functional Alterations of Human Induced Pluripotent Stem Cell-Derived Cardiomyocytes

Parvin Forghani, PhD[1]; Aysha Rashid, BS[2]; Fangxu Sun, PhD[3]; Rui Liu, BS[1]; Dong Li, PhD[1]; Megan R Lee, BS[1]; Hyun Hwang, BS[1]; Joshua T Maxwell, PhD[1]; Anant Mandawat, MD[4]; Ronghu Wu, PhD[3]; Khalid Salaita, PhD[2, 5]; Chunhui Xu, PhD[1, 5]

[1]Division of Pediatric Cardiology, Department of Pediatrics, Emory University School of Medicine and Children's Healthcare of Atlanta, Atlanta, GA 30332, USA

[2]Biomolecular Chemistry, Department of Chemistry, Emory University, Atlanta, GA 30332, USA

[4]Department of Biology, College of Sciences, Georgia Institute of Technology, Atlanta, GA 30332, USA

[3]School of Chemistry and Biochemistry and the Petit Institute for Bioengineering and Bioscience, Georgia Institute of Technology, Atlanta, GA 30332, USA

[4]Department of Medicine & Winship Cancer Institute, Emory University School of Medicine, Atlanta, GA 30322, USA

[5]Wallace H. Coulter Department of Biomedical Engineering, Georgia Institute of Technology and Emory University, Atlanta, GA 30332, USA

**Running Title:** Carfilzomib-induced Cardiotoxicity

**AHA Journals Subject Terms**: Basic, translational, and clinical research-Basic science research

Correspondence: Chunhui Xu, PhD, Associate Professor, Department of Pediatrics, Emory University School of Medicine, 2015 Uppergate Drive, Atlanta, GA 30322. Email: chunhui.xu@emory.edu; Tel: 404-727-7774

**Abstract**

**Background−** Anticancer therapies have significantly improved patient outcomes; however, cardiac side effects from cancer therapies remain a significant challenge. Cardiotoxicity following the treatment with proteasome inhibitors such as carfilzomib is known in clinical settings, but the underlying mechanisms have not been fully elucidated.

**Methods and Results−** Using human induced pluripotent stem cell-derived cardiomyocytes (hiPSC-CMs) as a cell model for drug-induced cytotoxicity in combination with traction force microscopy, functional assessments, high-throughput imaging, and comprehensive omic analyses, we examined the molecular mechanisms involved in structural and functional alterations induced by carfilzomib in hiPSC-CMs. Following the treatment of hiPSC-CMs with carfilzomib at 0.01 to 10 μM, we observed a concentration-dependent increase in carfilzomib-induced toxicity and corresponding morphological, structural and functional changes. Carfilzomib treatment reduced mitochondrial membrane potential, ATP production, and mitochondrial oxidative respiration and increased mitochondrial oxidative stress. In addition, carfilzomib treatment affected contractility of hiPSC-CMs in 3-dimensional (3D) microtissues. At a single cell level, carfilzomib treatment impaired $Ca^{2+}$ transients and reduced integrin-mediated traction forces as detected by piconewton tension sensors. Transcriptomic and proteomic analyses revealed that carfilzomib treatment downregulated the expression of genes involved in extracellular matrices, integrin complex and cardiac contraction and upregulated stress responsive proteins including heat shock proteins.

**Conclusions−** Carfilzomib treatment causes deleterious changes in cellular and functional characteristics of hiPSC-CMs. Insights into these changes could be gained from the changes in the expression of genes and proteins identified from our omic analyses.

**Key Words:** cardiomyocyte, cardiotoxicity, drug research, gene expression, stem cell

**Non-standard Abbreviations and Acronyms**

| | |
|---|---|
| **3D** | 3-dimensional |
| **Cfz** | carfilzomib |
| **ECM** | extracellular matrix |
| **DEGs** | differentially expressed genes |
| **DEPs** | differentially expressed proteins |
| **GO** | gene ontology |
| **hiPSC-CMs** | human induced pluripotent stem cell-derived cardiomyocytes |
| **HSPs** | heat shock proteins |
| **KEGG** | Kyoto encyclopedia of genes and genomes |
| **MFI** | mean fluorescence intensity |
| **OCR** | oxygen consumption rate |
| **qRT-PCR** | quantitative reverse transcription polymerase chain reaction |
| **RNA-seq** | RNA sequencing |
| **RICM** | reflection interference contrast microscopy |
| **ROS** | reactive oxygen species |
| **t-TGT** | turn on-tension gauge tether |
| **TMRM** | tetramethyl rhodamine methyl ester |

**Clinical Perspective**

What is new?

- Treatment of human stem cell-derived cardiomyocytes with carfilzomib resulted in oxidative stress, mitochondrial dysfunction, and cell death.
- Carfilzomib treatment negatively affected contractility, $Ca^{2+}$ handling and integrin-mediated traction forces in human stem cell-derived cardiomyocytes.
- Carfilzomib treatment downregulated the expression of genes involved in extracellular matrices, integrin complex and cardiac contraction and upregulated stress responsive proteins.

What are the clinical implications?

- Improving mitochondrial function, $Ca^{2+}$ handling, cardiac contraction, and integrin-mediated traction forces has the potential to mitigate carfilzomib-induced cardiotoxicity.
- The molecules such as heat shock proteins upregulated by carfilzomib treatment are potential biomarkers for carfilzomib-induced cardiotoxicity.

## Introduction

Anticancer therapies have significantly improved the outcomes of cancer patients over the past decade. However, several common chemotherapeutic agents including proteasome inhibitors are associated with an increased risk of arrhythmias, conduction abnormalities and other cardiac adverse events. Cardiac toxicities have been reported with FDA-approved proteasome inhibitors in clinical trials.[1] Carfilzomib (Cfz), a second-generation proteasome inhibitor for the treatment of relapsed or refractory multiple myeloma, can cause cardiotoxicity.[1-4] Clinical trials with Cfz have indicated cardiotoxicity including heart failure and cardiac arrhythmias.[5-7] A meta-analysis of 29 clinical trials including 4164 patients who received Cfz reported 8.6% and 4.9% incidence of all-grade and high-grade cardiotoxicity, respectively.[8] Another meta-analysis of 24 clinical trials including 2594 patients who received Cfz showed 18.1% and 8.2% incidence of all-grade and high-grade cardiotoxicity, respectively.[9] Although Cfz is used frequently in the treatment of multiple myeloma, the incidence of cardiotoxicity caused by Cfz appears to be higher than other proteasome inhibitors.[8]

Cfz has been well-characterized for its potent activity to irreversibly bind to and inhibit the chymotrypsin-like site of the proteasome,[10] blocking the ability of the ubiquitin/proteasome system to degrade and recycle misfolded or damaged proteins.[11] Cfz can effectively induce apoptosis and kill multiple types of human cancer cells with $IC_{50}$ ranging from 50 nM to 300 nM after 24 h exposure of cell cultures to Cfz.[12] Cardiomyocytes are also sensitive to proteasome inhibition possibly due to high protein turnover of contractile proteins.[11] For example, exposure of primary neonatal rat cardiomyocytes to submicromolar concentrations of Cfz induced apoptosis and myocyte damage.[13] A pre-clinical pharmacokinetics study identified chymotrypsin-like proteasomal activity of Cfz that can potentially damage rat cardiomyocytes at clinically relevant

concentrations.[14] However, cellular and molecular mechanisms underlying Cfz-induced cardiotoxicity remain to be fully elucidated.

As cardiovascular side effects of cancer therapies are increasing, the development of a human cell model is needed to facilitate the understanding of cardiotoxicity-related mechanisms. Progress in hiPSC-CM research has provided a new platform for the studies of drug-induced side effects and disease modeling.[15, 16] hiPSC-CMs have translational potential to improve current models by providing more precise and clinically relevant characteristics regarding responses to drug treatment.[17] They can also overcome the differences between human and animal cardiac physiology and challenges in long-term maintenance of primary human cardiomyocytes and can be engineered for scalable manufacture. Indeed, hiPSC-CMs have provided novel insights for the study of genetic heart diseases and drug responses.[18-20] Patient-specific hiPSC-CMs have also been used for pharmacogenetic studies to facilitate the identification of cancer survivors with increased risk of chemotherapy-related cardiomyopathy.[21]

To advance our understanding of the underlying mechanisms contributing to the Cfz-induced cardiotoxicity, here we provide a molecular and functional view of hiPSC-CMs post Cfz treatment. We found that Cfz induced dose-dependent cytotoxicity and targeted mitochondria at physiologically relevant doses, leading to the disruption of cellular energy and contractility. Additionally, we examined cellular function at the single cell level through traction force measurements using a nucleic acid-based tension sensor along with $Ca^{2+}$ transient imaging. Our findings on reduction in traction forces, abnormal $Ca^{2+}$ transients, mitochondrial dysfunction, and contractility impairment, in combination with comprehensive transcriptome and proteome analyses illustrate the possible molecular mechanisms in cardiomyocyte functional alteration post

Cfz treatment. Our study also provides a unique resource for the discovery of biomarkers associated with cardiomyocyte dysfunction and arrhythmias following Cfz therapy.

## Methods

### Data availability

Global gene expression profiling of RNA-seq (RNA sequencing) data are available at the NCBI Gene Expression Omnibus database with the accession number GSE163102. The proteomics data were deposited in the public MassIVE database with the identifier MSV000087350.

### Cardiomyocyte differentiation and spheroid formation

hiPSC lines SCVI-273 (Stanford Cardiovascular Institute) and IMR-90 (WiCell Research Institute) were differentiated toward cardiomyocytes using small molecules or growth factors based on previously published differentiation protocols[22, 23] (**Figure 1A**). hiPSC monolayers were dissociated using Versene (Thermo Fisher Scientific) and seeded onto 12-well plates coated with 1:60 Matrigel (Thermo Fisher Scientific). Cardiomyocyte differentiation was performed using 6 μMCHIR 99021 (Selleck Chemicals) in RPMI/B27 insulin-free medium (days 0-1) followed by 5 μM IWR-1 (Sigma-Aldrich) for two days on days 3-5. Medium was changed on day 5 and cells were maintained in RPMI/B27 with insulin for the remaining of days. In the second protocol, cells were treated with 100 ng/mL recombinant human activin A (R&D Systems) on day 0 and replaced with 10 ng/mL recombinant human bone morphogenic protein-4 (R&D Systems) in RPMI/B27 insulin-free medium from days 1 to 4. Differentiated cells were maintained in RPMI/B27 with insulin for 5 weeks with medium change every 2-3 days. Spheroids were generated using

AggreWell400 plates (1,800 cells per/microwell for each spheroids) from differentiated cultures on differentiation day 6 and maintained in RPMI/B27 with insulin.

SCVI-273 hiPSC-CMs were used for oxidative stress, caspase activity, mitochondrial membrane potential, ATP measurement, $Ca^{2+}$ transients, measurements of sarcomere length and cell structure, and RNA-seq analysis. IMR-90 hiPSC-CMs were used for qRT-PCR (quantitative reverse transcription polymerase chain reaction), traction force, contractility and proteomics analysis. Both hiPSC lines SCVI-273 and IMR90 derived CMs were used for cell viability and mitochondrial function with similar results and data from SCVI-273 hiPSC-CMs were presented.

**Assay to determine mitochondrial membrane potential**

To analyze changes in mitochondrial membrane potential in hiPSC-CMs, we used tetramethyl rhodamine methyl ester (TMRM), a dye probe which accumulates in mitochondria. Medium was removed following one day treatment with Cfz, and cells were labeled with 100 nM TMRM for 30 min at 37ºC. Cells were then counter stained with Hoechst (Thermo Fisher Scientific, H3570) and imaged immediately using ArrayScan XTI Live High Content Platform (Life Technologies).[24] We quantified the nuclear spots within the ring in channel 2 by using intensity as a readout.

**Drug preparation and treatment**

The stock solution of 10 mM Cfz (Selleck Chemicals, PR-171 and S2853) was prepared by dissolving 10 mg Cfz in 1.389 mL dimethyl sulfoxide (DMSO, Sigma-Aldrich) and stored at -80ºC. The peak plasma concentration based on pharmacokinetic characteristics of Cfz is 5.88 μM. A dose ranges from 0.01 to 10 μM was selected following initial testing of Cfz at 1, 2, 10 and 20 μM. To make 2X final concentration of Cfz in RPMI/B27 with insulin, drug dilution was

performed on the day of each experiment and kept on ice in the dark. DMSO at 0.2% (v/v), a concentration corresponding to the highest drug concentration, was used as vehicle control. Doxorubicin (Adriamycin, Selleck Chemicals) at 10 μM was used as a positive control for viability testing and 1 μM for contractility and $Ca^{2+}$ transient analysis. Stock solution of doxorubicin (10 mM) was made the same manner as Cfz. The peak plasma concentration of doxorubicin is 1.8-11 μM.

For the rescue experiment, hiPSC-CMs were pre-treated with ascorbic acid (Sigma-Aldrich) at 25 μg/mL for 2 h before the Cfz treatment and then treated with Cfz and ascorbic acid for 24 h before the analysis of cell viability by CellTiter-Blue assay (Promega). All treatments were adjusted to equivalent concentrations of DMSO (solvent).

***In vitro* cytotoxicity assays**

For monolayer culture of hiPSC-CMs, cell viability was measured using CellTiter-Blue assay (Promega). Monolayer cultures of hiPSC-CMs (IMR-90 and SCVI-273) were plated in Matrigel (1/60)-coated 96-well plates with clear bottom and black wall. Cells were allowed to attach at 37°C in RPMI-B27 with Rock inhibitor (10 μM) for 24 h prior to treatment with Cfz. Serially diluted Cfz was added to cells. After 24 and 48 h Cfz treatment, cells were incubated with 20 μL of the CellTiter-Blue reagent in 100 μL of RPMI/B27 medium solution for 2 h, the reduction of resazurin to resorufin in live cells was measured by fluorescence excitation at 530 nm and emission at 590 nm using BioTek micro-plate reader and Gen5 3.03 software. For 3D hiPSC-CMs, cell viability was measured by Live/Dead staining (Thermo Fisher Scientific). A master mix of 1 μM ethidium homodimer and 0.25 μM of calcein in RPMI/B27 medium was added following a wash with PBS. Cells were incubated for 25 min at 37˚C, washed twice with PBS and suspended in 5

ml of RPMI/B27 medium without Phenol red. Live/dead-stained cells were observed at 645 nm for ethidium homodimer and 530 nm for calcein-AM.

**Immunofluorescence staining**

hiPSC-CMs were dissociated with 0.05% Trypsin-EDTA and reseeded in Matrigel-coated 96-well culture plates at a density of $5\times10^4$ cells/well. Retrieved cells were fixed in 4% paraformaldehyde for 15 min following gentle PBS wash and permeabilized using 90% cold methanol for 2 min at room temperature. The cells were then blocked with 10% normal goat serum in PBS at room temperature for 1 h and incubated overnight at 4ºC with the primary antibodies against NKX2.5 (Cell Signaling, 1:1600) and α-actinin (Sigma-Aldrich, 1:800) diluted in 3% normal goat serum for the purity assay.[23] After the incubation with the primary antibodies, the cells were washed twice with PBS and incubated with secondary antibodies, Alexa Fluor 488-conjugated goat anti-mouse IgG1 (for α-actinin staining, Life Technologies) and Alexa Fluor 594-conjugated goat anti-rabbit IgG (for NKX2.5 staining, Life Technologies) diluted at 1:1000 in PBS with 0.25% BSA. The nuclei were counterstained with 7 μM Hoechst33342 (Thermo Fisher Scientific) for 15 min at room temperature and pre-imaged using an inverted microscope (Axio Vert.A1). Images of immunocytochemistry were quantitatively analyzed using ArrayScan XTI Live High Content Platform. The Cellomics Scan Software (Thermo Fisher Scientific) was used to capture images, data analysis was performed using Cellomics View Software (Thermo Fisher Scientific). Twenty fields/well were imaged using a 10x objective. Spot threshold was set to 10 units and detection limit was set at 25 units. The percentage of α-actinin-positive cells and the average intensity per well were used as readout.

**Caspase 3/7 detection**

Fresh Caspase-GloR 3/7 reagent (Promega) was reconstituted and added to cells as an indicator of apoptosis. Background readings were measured from wells containing culture medium without cells. Illuminometer readings were taken one hour after adding the Caspase-GloR 3/7 reagent.

**Assay to measure ATP content**

CellTiter-Glo 3D Cell Viability kit (Promega) was used to detect alterations in the cellular ATP content. 3D hiPSC-CMs were dissociated into single cells using 0.25% Trypsin-EDTA and replated into a 96-well plate at a density of $4.5x10^4$ cells/well. Medium was removed and RPMI without phenol red was added at 100 µL per well. The kit was thawed at 4°C a day before and the reagent was added at 100 µL per well (1:1 ratio) with 2 min shaking. Measurement was performed at Top Count NXT Microplate Luminescence Counter (PerkinElmer) with integration time of 1 second per well after 20 min incubation in room temperature.

**qRT-PCR**

Total RNA was extracted using Aurum total RNA mini kit (Bio-Rad) according to manufacturer's instructions. One µg total RNA was used for cDNA synthesis using the Superscript VILO cDNA synthesis kit (Thermo Fisher Scientific) and reaction mixture was incubated using a C1000 touch thermal cycler (Bio-Rad) as follows: 25℃ for 10 min, 37℃ for 2 h and 85℃ for 5 min. The reaction mixture was further diluted to 300 µL and 2 µL cDNA as template was subjected to qRT-PCR, which was performed in triplicates for each gene using a SYBR Green reaction master mix (Bio-Rad). Real-time PCR conditions included initial denaturation step at 95℃ for 10 min, 40 cycles of two-steps with 15 s of denaturation at 95℃ followed by 1 min of annealing at 60℃ using

Applied Biosystems 7500 real-time PCR systems. The mRNA levels of the genes examined were normalized to *GAPDH* mRNA levels. The primers used for the genes are listed in **Table 1**.

**Detection of mitochondrial reactive oxygen species (ROS)**

To analyze changes in mitochondrial ROS, we used MitoSOX Red (Thermo Fisher Scientific) staining. The cells were washed with PBS and incubated with 5 μM MitoSOX Red for 15 min at 37ºC and protected from light. Cells were counter-stained with Hoechst (Thermo Fisher Scientific) and imaged using ArrayScan XTI Live High Content Platform (Life Technologies).

**Seahorse extracellular flux analysis of mitochondrial respiration**

Seahorse plates were coated with Matrigel at 1/50 dilution one day before cell seeding. hiPSC-CMs were seeded at $2.5x10^5$ cells per well in 300 μL of the medium and were allowed to adhere for one day in a 37 °C humidified incubator with 5% $CO_2$. The Seahorse XF Sensor Cartridge was hydrated the day before by filling each well of the XF Utility plate with 1 mL of Seahorse XF Calibrant Solution and kept in a non-$CO_2$ 37°C incubator for 24 h to remove $CO_2$ from the media to prevent interference with pH-sensitive measurements. To pre-equilibrate, hiPSC-CMs were washed once with non-buffered RPMI supplemented with 10 mM glucose, 2 mM sodium pyruvate, and 2 mM glutamine. Cells were maintained in 525μL of XF Assay medium at 37 °C in a non-$CO_2$ incubator for 1 h. Agilent Seahorse XF24 Analyzer (Agilent Seahorse Bioscience) was used to analyze the mitochondrial function of the cells by sequential injections of modulators. A mixture of oligomycin (2 μM), carbonyl cyanide-4-(trifluoromethoxy) phenylhydrazone FCCP (1 μM), and rotenone (0.5 μM) were suspended in a pre-warmed XF Assay medium and loaded into the injection ports (75 μl) of the hydrated sensor cartridge corresponding to the order of injection.

Each measurement cycle consisted of 3 min of mixing, 2 min of waiting, and 3 min of measurements of oxygen consumption respiration. Measurement cycles were performed after each addition of the given compounds. The data was analyzed using Wave 2.6 and Report Generator Version: 4.0.

**$Ca^{2+}$ transient imaging**

Live cell imaging of intracellular $Ca^{2+}$ transients was performed with dye Fluo-4 AM (Thermo Fisher Scientific). Cells were incubated in Tyrode solution[25] containing Fluo-4 AM at a final concentration of 10 μM in the dark at 37°C for 20 min followed by a gentle wash at room temperature in pre-warm Tyrode solution. Fluorescence images were acquired using the Image Xpress Micro XLS System (Molecular Devices) with excitation/emission at 488/515-600 nm at a rate of 5 frames /sec and 10x magnification for four fields per well.

**Video-based contractility measurement**

Contractility of spontaneously beating hiPSC-CMs was recorded using a phase-contrast inverted microscope (Axio Vert.A1) equipped with Zeiss Axio Cam digital camera system.
Videos were recorded for 30 sec (5 frames/sec) under 10x magnification and were processed and exported using Zeiss AxioVision LE imaging software. Videos were converted to frame by frame image sequence using ImageJ. Video-based analysis of contractility was performed using MATLAB and motion vector software (R2016b, MathWorks Inc).[26]

**Probe preparation and traction force measurement**

Turn on-tension gauge tether (t-TGT) probes were used to measure molecular traction forces. DNA duplexes were conjugated to the fibronectin mimic cyclic-Arg-Gly-Asp-Phe-Lys (underline indicates *D* isomer) (cRGDfK), fluorophore (Cy3B), and quencher (BHQ) using previously published protocols.[27, 28] The duplex was tethered to a surface using biotin-streptavidin binding. When integrin receptors apply sufficient tension, the duplex will mechanically denature and specifically when the applied force exceeds the tension tolerance of the probe. The shearing TGT with a tension tolerance of 56 pN was used as described previously.[29] Glass surfaces were activated and functionalized with streptavidin. Next, biotinylated DNA tension probes were added. 3D hiPSC-CMs were treated with Cfz for one day, dissociated, and then re-seeded on the DNA-modified glass surfaces. Microscopy imaging of spontaneously contracting cells was performed using a Nikon TIRF microscope with 100x objectives.

**Measurements of sarcomere length and cell structure**

3D-derived hiPSC-CMs were treated with Cfz for one day, and then dissociated and re-seeded on the glass bottom microplates. Cells were stained with antibodies against α-actinin, and microscopy imaging was performed using a Nikon TIRF microscope in reflection interference contrast microscopy (RICM) and TRITC channels with 100X objectives. Image J software was used to quantify cell morphology, cell spread area, circularity, and aspect ratio. A program was written to obtain automated outlining of cells. To measure the z-lines, individual z-lines were selected, and lengths were measured per cell. For each cell, average length of ~20-30 z-lines was plotted.

**RNA-seq**

Total RNA was isolated from Day 30 hiPSC-CMs in biological triplicates following one day Cfz treatment using Aurum total RNA mini kit (Bio-Rad) according to the manufacturer's instructions. RNA concentrations were measured using Nanodrop Spectrophotometer (Thermo Fisher Scientific). Library prep and RNA sequencing was conducted by Novogene with 20 M reads per sample, PE150 Mapped Homo sapiens (GRCh38/hg38) to the genome using STAR (v2.6.1d) with ensemble annotation. Fastp was used for length limitation of adapter trimming (https://github.com/novogene-europe/fastp). The differentially expressed genes (DEGs) were used for analyses of GO (gene ontology) terms and KEGG (Kyoto encyclopedia of genes and genomes) pathways which were considered significantly enriched if the adjusted *P*-values < 0.05.

**Proteomic analysis**

Cells and culture media were collected from the triplicates of 3D hiPSC-CM cultures following one day Cfz treatment. Proteins were extracted from 3-4×$10^6$ hiPSC-CMs per sample by suspending the cells in the lysis buffer as described previously.[30] Proteins were purified through methanol-chloroform precipitation. For the secretome analysis, the media was passed through a filter (0.45 μm) and then concentrated by centrifugation (MW 3 kDa cutoff). Proteins were digested with trypsin overnight. Then purified peptides were labeled with the 6-plex TMT reagents for protein quantitation. The TMT-labeled samples (6 for the cell lysates and 6 for the secretomes) were mixed and fractionated. Each fraction was analyzed by liquid chromatography-tandem mass spectrometry. The data analyses were conducted as reported previously.[30]

**Statistical analysis and data presentation**

Statistical analyses were done using GraphPad Prism Version 8.00. Global differences were evaluated by Dunnett and Turkey test (One-Way ANOVA). *P*-value<0.05 was taken as statistically significant. *, *P*<0.05; **, *P*<0.01; ***, *P*<0.001; ****$P$<0.0001. Results are presented as mean ± SD in all experiments. Sample sizes are indicated in figure legends. For group comparison of gene expression in RNA-seq analysis, Benjamin-Hochberg correction was used to control false-discovery rate. We considered genes to be significantly differentially expressed between the two groups if adjusted *P*-value<0.05 and absolute value of $\log_2$(fold change)>1.

## Results

### Cfz treatment induced a dose- and duration-dependent cardiotoxicity

To examine whether Cfz treatment causes cytotoxicity in hiPSC-CMs, we generated enriched hiPSC-CMs (>90% NKX2.5-positive cells), treated the cells with various doses of Cfz, and characterized the cells 24 and 48 h post-treatment (**Figure 1A, B**). We used a common chemotherapeutic drug, doxorubicin, at 10 μM (a peak plasma concentration) as a control.[31] Following Cfz treatment, we observed dose- and duration-dependent increase of cell loss in Cfz-treated cultures compared with DMSO-treated cultures (**Figure 1C**). As detected by CellTiter Blue assay, cultures treated with Cfz at 10 μM and doxorubicin for 24 h had lower cell viabilities compared with cultures treated with DMSO. The cell viability in cultures treated with Cfz for 48 h began to decrease at doses as low as 0.1 μM, which is significantly lower than the peak concentration of the Cfz observed in patients' plasma after intravenous administration.[32, 33] Given that hiPSC-CM spheroids (3D cultures) provide a more physiologically relevant context for drug toxicity,[34] we examined whether Cfz could also induce cytotoxicity in 3D cultures. We generated hiPSC-CM spheroids using microscale tissue engineering [23] and treated them with Cfz

for 24 h. Using calcein and ethidium bromide as indicators for live and dead cells, respectively, we found that cultures treated with Cfz at 10 μM and doxorubicin had increased dead cells (ethidium bromide-positive cells) while moderate toxicity was also observed in cultures treated with Cfz at 0.1 and 1 μM (**Figure 1D**). These results suggest that Cfz induced dose-dependent cytotoxicity in both 2D and 3D cultures.

To determine the mechanism of cell death, we examined caspase3/7 activity using Caspase-Glo 3/7 Luminescent assay. Increased caspase3/7 activation was detected after Cfz treatment for 24 h, indicating that Cfz-induced cytotoxicity might be the result of apoptosis (**Figure 1E**).

**Cfz treatment increased mitochondrial superoxide and reduced mitochondrial function of hiPSC-CMs**

Oxidative stress through generation of mitochondrial superoxide and mitochondrial dysfunction plays important roles in cellular cytotoxicity,[35, 36] which could affect cardiac function.[37-39] We therefore examined the effect of Cfz treatment on mitochondrial oxidative stress and mitochondrial function. Based on fluorescence intensity of MitoSOX, a mitochondrial superoxide indicator, the relative levels of mitochondrial superoxide were higher in cultures treated with Cfz at 1 and 10 μM compared with DMSO-treated cultures (**Figure 1F**).

To examine if Cfz induced cytotoxicity through oxidative stress, we evaluated if ascorbic acid, a commonly used antioxidant, could rescue Cfz-induced cell loss. Compared with Cfz-treated cultures without ascorbic acid, the Cfz-treated cultures with ascorbic acid had significantly attenuated cell loss when cells were treated with Cfz at 0.01, 0.1 and 1 μM (**Figure 1G**), suggesting that Cfz-induced cytotoxicity is in part mediated by oxidative stress.

We also examined the effect of Cfz treatment on mitochondria membrane potential by staining the cells with tetramethylrhodamine, methyl ester (TMRM), a cell-permeant fluorescent dye that is sequestered by active mitochondria. hiPSC-CMs treated with Cfz at 0.1, 1, and 10 μM had more than 10-fold reduced levels of TMRM fluorescence intensity (**Figure 2A-B**). These results indicate a substantial decrease in mitochondrial membrane potential and increase in mitochondrial superoxide following Cfz treatment, suggesting that oxidative stress could play an important role in Cfz-mediated cardiac cytotoxicity.

To understand the effects of Cfz on mitochondrial function, we examined the expression of genes associated with mitochondrial function and performed Seahorse XF Cell Mito Stress test one day post Cfz treatment. Cfz treatment caused a dose-dependent decrease in the expression of genes associated with mitochondrial function, including *COQ10A, MFN1, MFN2,* and *NDUFB5,* but not *OPA1* and *UCP3* (**Figure 2C**). The basal and maximal respiratory capacity and ATP production (served as an indicator of mitochondrial function) were measured by monitoring oxygen consumption respiration after sequential injection of oligomycin, FCCP, and rotenone according to the manufacture's instruction. As shown in **Figure 2D-E**, a significant decrease in ATP production was detected following the treatment of Cfz at 0.1, 1 and 10 μM in SCVI-273 hiPSC-CMs. The reduced ATP levels were also observed in 3D cultures treated with Cfz as detected by CellTiter-Glo viability assay (**Figure 2F**). Higher concentrations of Cfz (10 μM) also decreased the basal and maximal mitochondrial respiration in SCVI-273 hiPSC-CMs (**Figure 2D-E**). Similarly, Cfz treatment reduced ATP production and basal mitochondrial respiration in IMR90 hiPSC-CMs (data not shown). These results suggest that Cfz induces mitochondrial damage and consequently the cardiotoxicity.

**Cfz treatment induced abnormal $Ca^{2+}$ transients and dysfunctional contractility**

There is increasing evidence that alteration in mitochondrial function results in increased ROS generation and abnormal $Ca^{2+}$ transients.[37, 40] Considering the link of oxidative stress and $Ca^{2+}$ transients, we analyzed the $Ca^{2+}$ transient profile 24 h post Cfz treatment. Cfz treatment of SCVI-273 hiPSC-CMs increased the proportion of cells with abnormal $Ca^{2+}$ transients (**Figure 3A**). Consistently, Cfz treatment decreased the expression of genes associated with $Ca^{2+}$ handling (*SLC8A1*, *RYR2*, *CASQ2*, and *ATP2A2*) (**Figure 3B**). The downregulation of these genes is consistent with the abnormal $Ca^{2+}$ transients following Cfz treatment. These results indicate that Cfz treatment impairs $Ca^{2+}$ transients at the single cell level, which may affect the contractility function of hiPSC-CMs.

To address if mitochondrial dysfunction along with abnormal $Ca^{2+}$ transients was associated with contractile dysfunction in Cfz-treated hiPSC-CMs, we assessed the contractility of 3D hiPSC-CM static spheroids after treatment with Cfz for 24 and 48 h using video microscopy with motion vector analysis. Cessations in contraction occurred in cultures treated with all concentrations (0.01, 0.1, 1, and 10 μM) of Cfz for 48 h. At 24 h post Cfz treatment, a portion of hiPSC-CM spheroids treated with Cfz at 0.01 μM or doxorubicin and all spheroids treated with 0.1, 1, and 10 μM stopped beating (**Figure 4A**). Similar results of cessations in contraction were observed in hiPSC-CMs derived from both SCVI-273 and IMR90 lines treated with Cfz at high doses. The average maximum contraction, maximum relaxation velocity, and the beat rate remained unchanged in the remaining beating cells from cultures treated with Cfz at 0.01 μM or doxorubicin compared with those from DMSO-treated cultures (**Figure 4B-C**). Additionally, Cfz reduced the expression of genes associated with contractility (*MYH6* and *MYL2)* (**Figure 4D**). These data suggest that Cfz increases contractile dysfunction in post-treatment.

**Cfz treatment reduced traction forces and caused structural disorganization**

To further examine the Cfz-induced alteration in contraction, we employed a DNA duplex TGT probe[29] to measure integrin-mediated traction forces in single cardiomyocytes. The TGT probe was modified with a fibronectin mimetic ligand (cyclic-RGD), fluorophore (Cy3B), and quencher. When cell integrins bind to the RGD ligand and transmit a threshold magnitude of tension greater than the probe's tension tolerance (56 pN), the duplex mechanically denatures, and the fluorophore separates from quencher. Because the biotin-anchored nucleic acid is also fluorescently tagged, shearing of the top strand leads to ~20-fold enhancement in fluorescence. Moreover, the fluorescence signal is directly proportional to the number of probes that experiences a threshold force exceeding 56 pN; therefore, the fluorescence signal provides a quantitative readout of integrin traction forces (**Figure 5A**). 3D hiPSC-CMs were treated with Cfz for one day, dissociated, and then re-seeded onto the glass surface with the TGT probe. We then quantified the fluorescence signal of single cardiomyocytes upon plating to monitor the traction forces of spontaneously contracting cardiomyocytes. As shown in **Figure 5B-C**, the traction forces of hiPSC-CMs decreased in cultures treated with Cfz at 0.01, 0.1, 1, and 10 μM or doxorubicin compared with DMSO-treated cells. Thus, Cfz reduced integrin-mediated traction forces.

To evaluate if structural changes were accompanied with the alteration in contraction induced by Cfz treatment, we measured cell structure of hiPSC-CMs post Cfz treatment by immunocytochemistry of α-actinin, a protein expressed in z-lines of cardiomyocytes. Cells treated with Cfz at 1 and 10 μM lacked clear *z*-lines, whereas the DMSO-treated cells and cells treated with Cfz at 0.01 and 0.1 μM had clear *z*-lines (**Figure 6A**). We also quantified cell size and shape along with sarcomere length to identify the link between the shape and contraction. Cells treated with higher concentrations of Cfz (1 and 10 μM) showed decreased cell area compared with

DMSO-treated cells; these cells also had irregular peripheral borders resulting in an increased circularity (**Figure 6B**). In addition, cells treated with Cfz at 0.01 and 0.1 μM or doxorubicin had shorter z-line length and sarcomere length compared with DMSO-treated cells (**Figure 6B**). These results indicate that Cfz treatment can induce significant structural alteration parallel with contractility dysfunction.

**Transcriptomic and proteomic analyses revealed that Cfz dysregulated genes related to stress response, extracellular matrix (ECM) and contractility**

To further elucidate the mechanism of Cfz-induced alteration in contractility, we compared global gene expression profile of hiPSC-CMs treated with Cfz at 1 μM for 24 h with DMSO-treated cells. RNA-seq analysis identified 5027 genes that were differentially expressed based on absolute $\log_2$ (fold change)>1 and adjusted $p<0.05$. Compared with DMSO-treated cells, 1913 genes were upregulated while 3114 genes were downregulated in Cfz-treated cells (**Figure 7A**). For example, Cfz induced downregulation of genes involved in cardiac muscle contraction (e.g., *ACTAA2*) and integrin complex (e.g., *ITGA11*). In addition, genes related to heat shock stress were upregulated, including *HSPA1b*, *HSPA16*, *HSPH1*, and *BAG3*, which participate in cellular response to stress, cell death, and apoptosis.

We also performed analysis of GO terms using the DEGs. GO terms related to oxidative stress, heat shock proteins (HSPs) and proteasomal protein catabolic process were upregulated, and GO terms related to ECM and cardiac contraction were downregulated (**Figure 7B, Table 2**). In line with Cfz-mediated mitochondrial oxidative stress, Cfz induced upregulation of GO terms including response to oxidative stress, reactive oxygen species metabolic process, response to temperature stimulus, and cellular response to heat. In contrast, Cfz induced downregulation of

GO terms of extracellular structure organization, extracellular matrix, actin binding, muscle system process, actin cytoskeleton, transmembrane receptor protein serine/threonine kinase signaling pathway, extracellular matrix structural constituent, contractile fiber, response to calcium ion, cardiac muscle contraction, and integrin binding and pathway-restricted SMAD protein phosphorylation.

The top downregulated genes based on fold change included those involved in integrin and ECM (*ITGAT1*, *MEGF6*, *FJX1*, *MAFP4*, *CCDC80*, and *FNDC10*), mitochondria (*SLIT3*, *DUT*, *PCK2*, and *ATP6VOE2*) and muscle contraction/tight junction (*ACTA2* and *SYNPO)* (**Table 3**). The top upregulated genes included genes involved in response to oxidative stress, heat stress, and reactive oxygen species metabolic process, including *HSPA1B*, *HSPA1A*, *DNAJA1*, *BAG3* and *HSP90AB1* (**Table 4**). Additionally, Cfz upregulated genes involved in MAP kinase-mediated signaling cascade (*MAP2K3*) and downregulated genes involved in SMAD pathway (*BMP10* and *BMP7*) (**Figure 7B**). Cfz also altered the expression of genes associated with ECM-receptor interaction, cell cycle, protein digestion and absorption, dilated cardiomyopathy, and hypertrophic cardiomyopathy (**Figure 7C**).

We further analyzed the DEGs based on z-scores. As shown in the heatmap (**Figure 7D**), the expression of genes related to cardiac muscle contraction was dramatically downregulated in Cfz-treated cells compared with DMSO-treated cells. These genes included response to calcium ion (*TNNT2*, *EEF2K*, *CARF*, *MYL3*, *MAP2K6*, *MYB*, *KCNJ5*, *KCNQ1*, *TNNT2*, *MYH7*, *RYR2*, and *CASQ2*), calcium responsive proteins (*RYR2*, *SLC25A12*, *CASQ2*, *WNT5A*, and *KCNMB1*), and contractile proteins (*SYNPO*, *ACTA2*, *FLNC, BMF*, *MYL3*, *MYO1D*, *ZNF185*, *TNNI1, TNNT3*, *MYL2*, *MYL5*, *MYLK*, *MYO5C*, *MYO15B*, *MYH6*, and *MYL7*). In addition, Cfz-dysregulated genes

were involved in ECM, integrin complex, and actinin cytoskeleton. These genes included *ITGA1*, *SYNPO*, *SLC6A4*, *CASQ2*, *TNNI1*, and *MYL3* (**Figure 7D**).

To examine the effect of Cfz at the protein level, we performed quantitative proteomic analysis on both the cell supernatant and cell lysate of hiPSC-CMs treated with Cfz at 1μM *vs*. DMSO for 24 h. Out of the 4060 proteins quantified in the cell lysate, 183 proteins were upregulated, and 39 proteins were downregulated (**Figure 8A**). Out of the 298 proteins detected in the cell supernatant, 6 proteins were upregulated, and 18 proteins were downregulated post Cfz treatment ($P$<0.05, absolute fold change>1.3) (**Figure 8B**). The downregulated proteins in the cell lysate included ANXA6 (a calcium-dependent membrane and phospholipid binding protein), SPTN1 (a filamentous cytoskeletal protein highly expressed in cardiac muscle at *z*-disc), and TPM1 (a protein forms a complex with troponin T and regulates actin-myosin interaction in response to intracellular $Ca^{2+}$ concentration).

As shown in **Figure 8A**, Cfz treatment reduced the expression of proteins in the cells associated with metabolic process, including PKM2 which is involved in glycolysis and regulates cardiomyocyte cell cycle, and PRKACA which is the catalytic subunit α of protein kinase A that contributes to the control of glucose metabolism and cell division. The downregulated proteins were associated with GO terms of metabolic process (PRKACA, SDHFA2, DHFAR, PGAM2, GOT1, IMPA1, CLEC16A, and ATM), mitochondrion organization (SDHFA2, GGCT, and MICOS1), striated muscle contraction (PRKACA, GSTM2, PGAM2, TPM1, and RCSD1), oxidation reduction (FDX1, HADH, IDH3G, PGAM2, PKM, TPI1, and SDHAF2), and muscle system process (ANXA, GSTM2, PGAM2, PRKAC, TPM1, and RCSD1) (**Figure 9A, Table 5**).

The enriched GO terms of upregulated proteins in the cells included cellular response to stress, ubiquitin-dependent protein catabolic process, protein folding, regulation of cellular

response to heat, cell death, and stress-activated mitogen-activated protein kinase cascade (**Figure 9B**). In addition, proteins associated with oxidative stress, autophagy, apoptosis and cell cycle were upregulated in the cells, including MAFG (a transcription factor which is induced following oxidative stress), ATG101 (an essential protein for the initiation of autophagy), RND3 (a member of the small Rho GTPase family that regulates apoptosis) and CDKN1A (**Figure 8A, Table 6**).

The downregulated proteins in the secretome included POSTN, CIS, THBS1, and COL3A1 (**Figure 8B, Table 7**). THBS1 is an adhesive glycoprotein that mediates cell-to-cell and cell-to-ECM interactions; COL3A1 provides instructions for making type III collagen that strengthens and supports cardiac tissue; and POSTN is a ligand for integrins providing the support for cell adhesion. The downregulated proteins in secretome are associated with GO terms including extracellular matrix organization, cell-matrix adhesion, and cell motility (**Figure 9C**) and KEGG pathways including tight junction and DNA replication (**Table 8**). In addition, upregulation of HSPs and chaperons was observed in both the cells and the secretome, including HSPA1A, HSPH1, DnaJ A&B (HSP40); ZFAND2A, and CRYAB (**Figure 8A-B, Table 7)**.

Comparison of the proteomic and transcriptomic data revealed a set of overlapping genes and proteins that were differentially expressed in response to Cfz treatment (**Figure 8C-D**). We performed additional GO-term analysis using these overlapping genes and proteins (**Figure 8E, Table 9**). The enriched GO terms included response to heat, HSP binding, and ATPase regulator activity (**Figure 8E**). Several pathways were upregulated, including apoptotic signaling (*ATF3*, *CDKN1A, DNAJA1, HSPA1A, SERPINE1, BAG3,* and *USP47*), stress-activated mitogen-activated protein kinase cascade (*CRYAB*, *HMGCR*, *DNAJA1*, *SKP1*, and *UBB*) and ATPase activity (*DNAJA*, *DNAJB1*, *BAG*3, *HSPH1*, and *DNAJB4*) (**Table 9**). We note that RNA-seq was analyzed using hiPSC-CMs derived from SCVI-273 line and proteomics analysis was performed using

hiPSC-CMs derived from IMR-90 hiPSCs. The consistency in the alterations in the expression of these overlapping genes and proteins in two cell lines suggests that the observed alterations induced by Cfz treatment are independent of the cell lines used.

In addition, Cfz treatment upregulated several ubiquitin-related proteins. As detected by RNA-seq, ubiquitin C was among the top 20 upregulated proteins (**Table 4**). Proteomic analysis of cell lysates also revealed that several ubiquitin-related proteins were upregulated, including negative regulator of ubiquitin like proteins 1, praja ring finger ubiquitin ligase 2, ubiquitin specific peptidase 33, and ubiquitin B (**Table 6**). GO-term analysis of differentially expressed proteins (DEPs) identified ubiquitin protein ligase binding (n = 44) and ubiquitin dependent ERAD pathway (n = 16). These changes may indicate the direct effect of Cfz on the ubiquitin-proteasome pathway.

Taken together, the transcriptomic and proteomic analyses of hiPSC-CMs indicate that downregulation of contractile related genes/proteins, and ECM and integrin-related genes/proteins together with upregulation of HSPs and stress-activated pathways were associated with cardiac toxic effects of Cfz treatment.

## Discussion

Using molecular tension sensors to quantify cellular traction forces in combination with high-throughput imaging, functional assessments, and transcriptomic and proteomic analyses, we investigated mechanisms of earlier cellular and molecular events associated with alterations of contraction post Cfz treatment in hiPSC-CMs. Our results suggest a possible role of ECM and integrin-related genes in contractility and traction force defects as an early response to Cfz treatment. We also identified increased mitochondrial oxidative stress, reduced mitochondrial

function, abnormal $Ca^{2+}$ transients and changes in the sarcomere structure and cell morphology that might impact the contractile potency and traction forces of hiPSC-CMs post Cfz treatment. Transcriptomic and proteomic analyses highlighted an important role of the genes involved in ECM signaling including integrin and actin filaments. In parallel, our study revealed an increase in genes associated with stress response (e.g., HSPs). These results suggest that cardiotoxicity can result from the cumulative response to both 'off-target' and 'on-target' effects of Cfz treatment.

Since the FDA approval of Cfz in 2012, there has been increasing evidence surrounding Cfz-associated adverse cardiovascular events including cardiac arrest and cardiac arrhythmias.[1, 3, 4, 6] Cfz is also considered as an approved drug with repurposing potential for mechano-based therapeutic interventions,[41] although integrin-mediated contraction alteration of cardiomyocytes post Cfz treatment has not yet been characterized. This is the first study that applies a piconewton tension sensor to examine cytotoxic effects of Cfz on hiPSC-CMs. Using the TGT probes, we found that Cfz decreased integrin-mediated traction forces of hiPSC-CMs as measured by changes in fluorescence intensity on the probes due to contraction of individual cells. Our study provides a new avenue of mechano-pharmacology platform to study the impact of Cfz at molecular and cellular levels.

Recent evidence illustrates off-target effects of Cfz treatment in animal models; however, mechanisms underlying contraction alteration post Cfz treatment in cardiomyocytes have not been fully characterized. Our findings indicate the possibility of on-target and off-target effects of Cfz on human cardiac cells. Using RNA-seq, we identified early transcriptomic signatures of Cfz-induced cardiotoxicity and important genes/pathways that might mediate Cfz-induced cell death and contraction defects. Following a 24 h treatment of hiPSC-CMs with Cfz, there was significant upregulation of genes and related proteins involved in cellular stress. In particular, RNA-seq

revealed that Cfz treatment induced the overexpression of genes encoding HSPs including *HSPA1B, HSPA1A,* and *HSPA6.* Consistent with our RNA-seq data, the proteomic analysis also confirmed upregulation of HSPs in both the cell lysate and the secretome, including HSP90, HSPAB1, and HSPAA1 as well as molecules that act as co-chaperones including DnaJ A&B (HSP40), HSPH1, ZFAND2A, and CRYAB. It has been reported that proteasome inhibitors such as bortezomib can upregulate HSPs,[42] and targeting HSPs has been considered to overcome resistance to chemotherapeutic agents such as imatinib and cisplatin.[43] HSP90 has been found to assist in degrading toxic metabolites by promoting ubiquitination and proteasome lysis.[44] Overexpression of HSPs is also linked to many pathological conditions[45, 46] and increased HSPs have a protective function by blocking apoptosis, which allows cells to survive in otherwise lethal conditions [47, 48]. It is likely that increased HSPs may overcome the toxic effect of the inhibition of proteasomes post Cfz treatment in hiPSC-CMs. Given that increased HSPs are detectable in the secretome following the Cfz treatment, these HSPs may serve as biomarkers for early detection of Cfz-induced cardiotoxicity.

Our results highlight the possible role of the ECM and integrins in contractility defects as an early response to Cfz treatment. Alterations in ECM can impact cardiomyocyte function.[49, 50] Indeed, ECM and secreted proteins are important components of the stroma, which could play important roles in the cell-cell communication and regulation of cell process including contraction.[51] Integrins are sensors that transmit mechanical signals to ion channels.[52] The results of the GO term analysis indicate that genes belong to the ECM, integrin complex and actinin cytoskeleton proteins were downregulated in Cfz-treated cells. Cfz treatment also downregulated genes associated with cardiac muscle cell contraction, including contractile proteins (e.g., MYL2 and MYH6) and $Ca^{2+}$ handing proteins. In line with RNA-seq data, our proteome data in both cell

lysate and secretome also indicate significant reduction of proteins related to both contraction and ECM including POSTN, COL3A1, Thrombospondin 1, CIS, ANXA6, and TPM.

The current results demonstrate that Cfz interferes with mitochondrial function as indicated by reduced ATP production and respiration, increased mitochondrial ROS, and decreased mitochondrial membrane potentials. The reduced mitochondrial function and cellular energy impairment may contribute to cardiomyocyte dysfunction, which is consistent with previously published *in vivo* off-target effects of Cfz.[53] Increased mitochondrial ROS is known to be associated with cytotoxicity. [35, 38, 54] We also found similar results of increased mitochondrial ROS by treating hiPSC-CMs with doxorubicin, a cancer therapy drug with well-known cardiovascular toxicity effect due to the generation of ROS,[55, 56] reduced contractile capacity,[57]and adverse effect on $Ca^{2+}$ transport.[31] The increased mitochondrial ROS and decreased mitochondrial function in Cfz-treated hiPSC-CMs were also associated with the downregulation of genes associated with mitochondrial function such as NADH ubiquinone oxidoreductase subunit AB1, which is a crucial regulator of mitochondrial energy and ROS metabolism through coordinating the assembly of respiratory complexes.[58] In addition, our proteomic analysis indicated downregulation of SDHFA2, a member of succinate dehydrogenase complex, which plays essential roles in both the mitochondrial electron transport chain and the tricarboxylic acid cycle.

Consistent with the findings on increased mitochondrial oxidative stress, defects in mitochondrial function, and increased gene expression and proteins related to response to oxidative stress in Cfz-treated hiPSC-CMs, we found that cell death in Cfz-treated hiPSC-CMs could be rescued by targeting oxidative stress with ascorbic acid. These results suggest that oxidative stress plays an important role in Cfz-induced cytotoxicity and that antioxidants have the potential for cardioprotective therapy.

The Cfz-induced mitochondrial changes may lead to other functional alterations including abnormal $Ca^{2+}$ signaling. On the other hand, abnormal $Ca^{2+}$ signaling can induce alterations in respiratory chain complexes, which lead to increased mitochondrial oxidative stress and reduced mitochondrial membrane potential.[35, 37] Our results showed a significant increase in $Ca^{2+}$ transient abnormalities post Cfz treatment, which is consistent with clinical observations showing arrhythmias post chemotherapeutic drugs as a common phenomenon.[40, 59] In pathological conditions, $Ca^{2+}$ overload is accompanied by alterations in mitochondrial function and mitochondrial membrane potential[37, 38, 60] and abnormal $Ca^{2+}$ transients can be an indicator for pro-arrhythmic behavior of cardiomyocytes.[61] In cardiomyocytes, the interplay between $Ca^{2+}$ signaling and mitochondrial function is necessary to maintain normal cardiac function.[22, 37] Cfz treatment of hiPSC-CMs significantly downregulated several genes encoding $Ca^{2+}$ handling proteins, including *RYR2* and *CASQ2*, which play a critical role in excitation–contraction coupling in cardiomyocytes. Consistently, Cfz treatment increased abnormal $Ca^{2+}$ transients in hiPSC-CMs. Our findings support that possible mechanisms of Cfz-induced cardiotoxicity are associated with abnormal $Ca^{2+}$ signaling and mitochondrial oxidative stress, contributing to the development of arrhythmias post Cfz treatment.

We also found that Cfz treatment reduced the expression of proteins associated with metabolic process. For example, Cfz reduced the expression of glucose metabolism-related enzymes including PKM2 and PRKACA. Loss of function studies show that *PKM2* deletion in cardiomyocytes resulted in significantly reduced cell cycle.[62] PRKACA is a key regulatory enzyme in humans and contributes to the control of cellular processes including glucose metabolism and cell division. Defective regulation of protein kinase A activity is also linked to the progression of cardiovascular disease, and reduced protein kinase A activity is associated with

reduction of $Ca^{2+}$ signaling in embryonic hearts.[63] In addition, Cfz dysregulated the expression of proteins involved in autophagy, apoptosis and cell cycle. For example, Cfz downregulated CLEC16A, a regulator of autophagy through mTOR activity,[64] and upregulated ATG101 (an autophagy factor required for autophagosome formation), CDKN1A (a regulator of cell cycle in response to stress stimuli) and RND3 (a member of the small Rho GTPase family that regulates apoptosis through the Rho kinase-dependent signaling pathway).

Considering the complexity of cardiotoxicity, several possible mechanisms can synergistically induce cytotoxic effects post Cfz treatment. As expected from its on-target effect, proteasome inhibition by Cfz treatment can promote cell death. Our study also reveals potential novel mechanisms induced by Cfz-treatment, including (1) targeting mitochondria that may lead to oxidative stress, disruptions in cellular energy and contractility defect; and (2) triggering downregulation of ECM and integrin-related genes that may result in reduced integrin-mediated traction forces and alterations of cell structure and morphology.

We note that a replication study in human patients is an important next step to examine if the alterations of genes and proteins observed in hiPSC-CMs are also observed in human patients. However, given the similar endpoints observed in hiPSC-CMs and human patients (e.g., cytotoxicity and abnormal contractility), the findings of hiPSC-CMs from this study may have important implications towards discovery of new therapies to overcome clinical side effects post chemotherapeutic drug treatment. In addition, molecular changes such as upregulation of heat shock-related genes and other proteins may provide a new avenue towards biomarker development for early detection of Cfz-induced cardiotoxicity.

**Sources of Funding**

This study was supported by the Children's Heart Research and Outcomes Center at Emory University and Children's Healthcare of Atlanta; the Center for Pediatric Technology and Biolocity at Emory University and Georgia Institute of Technology; Imagine, Innovate and Impact (I3) Funds from the Emory School of Medicine and through the Georgia Clinical and Translational Science Awards (CTSA) Program (the National Institutes of Health award) [UL1-TR002378]; the National Institutes of Health [R21AA025723, R01HL136345, and R01AA028527]; and the National Science Foundation and the Center for Advancement of Science in Space [CBET 1926387].

**Conflict of Interest Disclosures**

None.

**Author Contributions**

P.F., A.M., and C.X. conceived and designed research. P.F., A.R., F.S., M.R.L., and D.L. performed research and acquired the data. P.F., A.R., F.S., R.L., M.R.L, D.L., H.H., and J.T.M. analyzed and interpreted the data. P.F., F.S., and R.L. performed statistical analysis. A.M. provided clinical guidance. R.W. and K.S. contributed new reagents or analytic tools, interpreted the data, and made critical revision of the manuscript for important intellectual content. P.F. and C.X. wrote the manuscript and made critical revision of the manuscript for important intellectual content. C.X. handled funding and supervision.

## References


1. Cole DC, Frishman WH. Cardiovascular complications of proteasome inhibitors used in multiple myeloma. *Cardiol Rev*. 2018;26:122-129
2. Kuhn DJ, Chen Q, Voorhees PM, Strader JS, Shenk KD, Sun CM, Demo SD, Bennett MK, van Leeuwen FW, Chanan-Khan AA, et al. Potent activity of carfilzomib, a novel, irreversible inhibitor of the ubiquitin-proteasome pathway, against preclinical models of multiple myeloma. *Blood*. 2007;110:3281-3290
3. Dimopoulos MA, Roussou M, Gavriatopoulou M, Psimenou E, Ziogas D, Eleutherakis-Papaiakovou E, Fotiou D, Migkou M, Kanellias N, Panagiotidis I, et al. Cardiac and renal complications of carfilzomib in patients with multiple myeloma. *Blood Adv*. 2017;1:449-454
4. Mangla A, Paydary K, Liu J, Mbachi C, Yim B, Lad TE. Carfilzomib-associated cardiovascular adverse events in a non-caucasian cohort of patients with multiple myeloma: A real-world experience. *Hematol Oncol*. 2018;36:715-717
5. Moreau P, Richardson PG, Cavo M, Orlowski RZ, San Miguel JF, Palumbo A, Harousseau JL. Proteasome inhibitors in multiple myeloma: 10 years later. *Blood*. 2012;120:947-959
6. Jain T, Narayanasamy H, Mikhael J, Reeder CB, Bergsagel PL, Mayo A, Stewart AK, Mookadam F, Fonseca R. Systolic dysfunction associated with carfilzomib use in patients with multiple myeloma. *Blood Cancer J*. 2017;7:642
7. Bruno G, Bringhen S, Maffei I, Iannaccone A, Crea T, Ravera A, Astarita A, Vallelonga F, Salvini M, Gay F, et al. Cardiovascular organ damage and blood pressure levels predict adverse events in multiple myeloma patients undergoing carfilzomib therapy. *Cancers (Basel)*. 2019;11
8. Shah C, Bishnoi R, Jain A, Bejjanki H, Xiong S, Wang Y, Zou F, Moreb JS. Cardiotoxicity associated with carfilzomib: Systematic review and meta-analysis. *Leuk Lymphoma*. 2018;59:2557-2569
9. Waxman AJ, Clasen S, Hwang WT, Garfall A, Vogl DT, Carver J, O'Quinn R, Cohen AD, Stadtmauer EA, Ky B, et al. Carfilzomib-associated cardiovascular adverse events: A systematic review and meta-analysis. *JAMA Oncol*. 2018;4:e174519
10. Kortuem KM, Stewart AK. Carfilzomib. *Blood*. 2013;121:893-897
11. Hahn VS, Zhang KW, Sun L, Narayan V, Lenihan DJ, Ky B. Heart failure with targeted cancer therapies: Mechanisms and cardioprotection. *Circ Res*. 2021;128:1576-1593
12. Han B, Yao W, Oh YT, Tong JS, Li S, Deng J, Yue P, Khuri FR, Sun SY. The novel proteasome inhibitor carfilzomib activates and enhances extrinsic apoptosis involving stabilization of death receptor 5. *Oncotarget*. 2015;6:17532-17542
13. Hasinoff BB, Patel D, Wu X. Molecular mechanisms of the cardiotoxicity of the proteasomal-targeted drugs bortezomib and carfilzomib. *Cardiovasc Toxicol*. 2017;17:237-250
14. Efentakis P, Kremastiotis G, Varela A, Nikolaou PE, Papanagnou ED, Davos CH, Tsoumani M, Agrogiannis G, Konstantinidou A, Kastritis E, et al. Molecular mechanisms of carfilzomib-induced cardiotoxicity in mice and the emerging cardioprotective role of metformin. *Blood*. 2019;133:710-723
15. Musunuru K, Sheikh F, Gupta RM, Houser SR, Maher KO, Milan DJ, Terzic A, Wu JC, American Heart Association Council on Functional G, Translational B, et al. Induced pluripotent stem cells for cardiovascular disease modeling and precision medicine: A

scientific statement from the american heart association. *Circ Genom Precis Med*. 2018;11:e000043
16. Mordwinkin NM, Burridge PW, Wu JC. A review of human pluripotent stem cell-derived cardiomyocytes for high-throughput drug discovery, cardiotoxicity screening, and publication standards. *J Cardiovasc Transl Res*. 2013;6:22-30
17. Hnatiuk AP, Briganti F, Staudt DW, Mercola M. Human ipsc modeling of heart disease for drug development. *Cell Chem Biol*. 2021;28:271-282
18. Bellin M, Mummery CL. Inherited heart disease - what can we expect from the second decade of human ips cell research? *FEBS Lett*. 2016;590:2482-2493
19. Mercola M, Colas A, Willems E. Induced pluripotent stem cells in cardiovascular drug discovery. *Circ Res*. 2013;112:534-548
20. Nair P, Prado M, Perea-Gil I, Karakikes I. Concise review: Precision matchmaking: Induced pluripotent stem cells meet cardio-oncology. *Stem Cells Transl Med*. 2019;8:758-767
21. Singh P, Wang X, Hageman L, Chen Y, Magdy T, Landier W, Ginsberg JP, Neglia JP, Sklar CA, Castellino SM, et al. Association of gstm1 null variant with anthracycline-related cardiomyopathy after childhood cancer-a children's oncology group alte03n1 report. *Cancer*. 2020;126:4051-4058
22. Lan F, Lee AS, Liang P, Sanchez-Freire V, Nguyen PK, Wang L, Han L, Yen M, Wang Y, Sun N, et al. Abnormal calcium handling properties underlie familial hypertrophic cardiomyopathy pathology in patient-specific induced pluripotent stem cells. *Cell Stem Cell*. 2013;12:101-113
23. Jha R, Wu Q, Singh M, Preininger MK, Han P, Ding G, Cho HC, Jo H, Maher KO, Wagner MB, et al. Simulated microgravity and 3d culture enhance induction, viability, proliferation and differentiation of cardiac progenitors from human pluripotent stem cells. *Sci Rep*. 2016;6:30956
24. Billis P, Will Y, Nadanaciva S. High-content imaging assays for identifying compounds that generate superoxide and impair mitochondrial membrane potential in adherent eukaryotic cells. *Curr Protoc Toxicol*. 2014;59:25 21 21-14
25. Rampoldi A, Crooke SN, Preininger MK, Jha R, Maxwell J, Ding L, Spearman P, Finn MG, Xu C. Targeted elimination of tumorigenic human pluripotent stem cells using suicide-inducing virus-like particles. *ACS Chem Biol*. 2018;13:2329-2338
26. Huebsch N, Loskill P, Mandegar MA, Marks NC, Sheehan AS, Ma Z, Mathur A, Nguyen TN, Yoo JC, Judge LM, et al. Automated video-based analysis of contractility and calcium flux in human-induced pluripotent stem cell-derived cardiomyocytes cultured over different spatial scales. *Tissue Eng Part C Methods*. 2015;21:467-479
27. Gao W, Shi P, Chen X, Zhang L, Liu J, Fan X, Luo X. Clathrin-mediated integrin alphaiibbeta3 trafficking controls platelet spreading. *Platelets*. 2018;29:610-621
28. Liu Y, Blanchfield L, Ma VP, Andargachew R, Galior K, Liu Z, Evavold B, Salaita K. DNA-based nanoparticle tension sensors reveal that t-cell receptors transmit defined pn forces to their antigens for enhanced fidelity. *Proc Natl Acad Sci U S A*. 2016;113:5610-5615
29. Ma R, Kellner AV, Ma VP, Su H, Deal BR, Brockman JM, Salaita K. DNA probes that store mechanical information reveal transient piconewton forces applied by t cells. *Proc Natl Acad Sci U S A*. 2019;116:16949-16954

30. Liu R, Sun F, Forghani P, Armand LC, Rampoldi A, Li D, Wu R, Xu C. Proteomic profiling reveals roles of stress response, ca(2+) transient dysregulation, and novel signaling pathways in alcohol-induced cardiotoxicity. *Alcohol Clin Exp Res*. 2020;44:2187-2199
31. Hanna AD, Lam A, Tham S, Dulhunty AF, Beard NA. Adverse effects of doxorubicin and its metabolic product on cardiac ryr2 and serca2a. *Mol Pharmacol*. 2014;86:438-449
32. Takemura G, Fujiwara H. Doxorubicin-induced cardiomyopathy from the cardiotoxic mechanisms to management. *Prog Cardiovasc Dis*. 2007;49:330-352
33. Maillet A, Tan K, Chai X, Sadananda SN, Mehta A, Ooi J, Hayden MR, Pouladi MA, Ghosh S, Shim W, et al. Modeling doxorubicin-induced cardiotoxicity in human pluripotent stem cell derived-cardiomyocytes. *Sci Rep*. 2016;6:25333
34. Polonchuk L, Chabria M, Badi L, Hoflack JC, Figtree G, Davies MJ, Gentile C. Cardiac spheroids as promising in vitro models to study the human heart microenvironment. *Sci Rep*. 2017;7:7005
35. Starkov AA. The role of mitochondria in reactive oxygen species metabolism and signaling. *Ann N Y Acad Sci*. 2008;1147:37-52
36. Bernardi P, Di Lisa F, Fogolari F, Lippe G. From atp to ptp and back: A dual function for the mitochondrial atp synthase. *Circ Res*. 2015;116:1850-1862
37. Brookes PS, Yoon Y, Robotham JL, Anders MW, Sheu SS. Calcium, atp, and ros: A mitochondrial love-hate triangle. *Am J Physiol Cell Physiol*. 2004;287:C817-833
38. Indo HP, Davidson M, Yen HC, Suenaga S, Tomita K, Nishii T, Higuchi M, Koga Y, Ozawa T, Majima HJ. Evidence of ros generation by mitochondria in cells with impaired electron transport chain and mitochondrial DNA damage. *Mitochondrion*. 2007;7:106-118
39. Sabharwal SS, Schumacker PT. Mitochondrial ros in cancer: Initiators, amplifiers or an achilles' heel? *Nat Rev Cancer*. 2014;14:709-721
40. Buza V, Rajagopalan B, Curtis AB. Cancer treatment-induced arrhythmias: Focus on chemotherapy and targeted therapies. *Circ Arrhythm Electrophysiol*. 2017;10
41. Lampi MC, Reinhart-King CA. Targeting extracellular matrix stiffness to attenuate disease: From molecular mechanisms to clinical trials. *Sci Transl Med*. 2018;10
42. Shah SP, Nooka AK, Jaye DL, Bahlis NJ, Lonial S, Boise LH. Bortezomib-induced heat shock response protects multiple myeloma cells and is activated by heat shock factor 1 serine 326 phosphorylation. *Oncotarget*. 2016;7:59727-59741
43. Lu XY, Xiao L, Wang L, Ruden DM. Hsp90 inhibitors and drug resistance in cancer: The potential benefits of combination therapies of hsp90 inhibitors and other anti-cancer drugs. *Biochemical Pharmacology*. 2012;83:995-1004
44. Pratt WB, Morishima Y, Peng HM, Osawa Y. Proposal for a role of the hsp90/hsp70-based chaperone machinery in making triage decisions when proteins undergo oxidative and toxic damage. *Exp Biol Med (Maywood)*. 2010;235:278-289
45. Kamal A, Boehm MF, Burrows FJ. Therapeutic and diagnostic implications of hsp90 activation. *Trends Mol Med*. 2004;10:283-290
46. Hoter A, El-Sabban ME, Naim HY. The hsp90 family: Structure, regulation, function, and implications in health and disease. *Int J Mol Sci*. 2018;19
47. Creagh EM, Sheehan D, Cotter TG. Heat shock proteins--modulators of apoptosis in tumour cells. *Leukemia*. 2000;14:1161-1173
48. Lanneau D, Brunet M, Frisan E, Solary E, Fontenay M, Garrido C. Heat shock proteins: Essential proteins for apoptosis regulation. *J Cell Mol Med*. 2008;12:743-761

49. Boothe SD, Myers JD, Pok S, Sun J, Xi Y, Nieto RM, Cheng J, Jacot JG. The effect of substrate stiffness on cardiomyocyte action potentials. *Cell Biochem Biophys*. 2016;74:527-535
50. Tallawi M, Rai R, Boccaccini AR, Aifantis KE. Effect of substrate mechanics on cardiomyocyte maturation and growth. *Tissue Eng Part B Rev*. 2015;21:157-165
51. Schelbert EB, Fonarow GC, Bonow RO, Butler J, Gheorghiade M. Therapeutic targets in heart failure: Refocusing on the myocardial interstitium. *J Am Coll Cardiol*. 2014;63:2188-2198
52. Becchetti A, Petroni G, Arcangeli A. Ion channel conformations regulate integrin-dependent signaling. *Trends Cell Biol*. 2019;29:298-307
53. Moreb JS. Off-target effects of carfilzomib that cause cardiotoxicity. *Blood*. 2019;133:626-628
54. Raturi A, Simmen T. Where the endoplasmic reticulum and the mitochondrion tie the knot: The mitochondria-associated membrane (mam). *Biochim Biophys Acta*. 2013;1833:213-224
55. Arai M, Yoguchi A, Takizawa T, Yokoyama T, Kanda T, Kurabayashi M, Nagai R. Mechanism of doxorubicin-induced inhibition of sarcoplasmic reticulum ca(2+)-atpase gene transcription. *Circ Res*. 2000;86:8-14
56. Berthiaume JM, Wallace KB. Adriamycin-induced oxidative mitochondrial cardiotoxicity. *Cell Biol Toxicol*. 2007;23:15-25
57. Dimitrakis P, Romay-Ogando MI, Timolati F, Suter TM, Zuppinger C. Effects of doxorubicin cancer therapy on autophagy and the ubiquitin-proteasome system in long-term cultured adult rat cardiomyocytes. *Cell Tissue Res*. 2012;350:361-372
58. Hou T, Zhang R, Jian C, Ding W, Wang Y, Ling S, Ma Q, Hu X, Cheng H, Wang X. Ndufab1 confers cardio-protection by enhancing mitochondrial bioenergetics through coordination of respiratory complex and supercomplex assembly. *Cell Res*. 2019;29:754-766
59. Guglin M, Aljayeh M, Saiyad S, Ali R, Curtis AB. Introducing a new entity: Chemotherapy-induced arrhythmia. *Europace*. 2009;11:1579-1586
60. Sauer H, Wartenberg M, Hescheler J. Reactive oxygen species as intracellular messengers during cell growth and differentiation. *Cell Physiol Biochem*. 2001;11:173-186
61. Filice D, Dhahri W, Solan JL, Lampe PD, Steele E, Milani N, Van Biber B, Zhu WZ, Valdman TS, Romagnuolo R, et al. Optical mapping of human embryonic stem cell-derived cardiomyocyte graft electrical activity in injured hearts. *Stem Cell Res Ther*. 2020;11:417
62. Magadum A, Singh N, Kurian AA, Munir I, Mehmood T, Brown K, Sharkar MTK, Chepurko E, Sassi Y, Oh JG, et al. Pkm2 regulates cardiomyocyte cell cycle and promotes cardiac regeneration. *Circulation*. 2020;141:1249-1265
63. Sui X, Kong N, Ye L, Han W, Zhou J, Zhang Q, He C, Pan H. P38 and jnk mapk pathways control the balance of apoptosis and autophagy in response to chemotherapeutic agents. *Cancer Lett*. 2014;344:174-179
64. Tam RC, Li MW, Gao YP, Pang YT, Yan S, Ge W, Lau CS, Chan VS. Human clec16a regulates autophagy through modulating mtor activity. *Exp Cell Res*. 2017;352:304-312

**Figure Legends**

**Figure 1**. **Cfz treatment induced dose-dependent cytotoxicity in hiPSC-CMs.** (**A**) Overall experimental design. **(B**) Representative images of immunofluorescence staining for examining cardiac purity using NKX2.5 antibodies and cardiomyocyte purity (% NKX 2.5-positive cells) of 3D hiPSC-CMs following the treatment with Cfz analyzed by ArrayScan**. (C)** Relative cell viability of hiPSC-CMs 24 and 48 h post Cfz treatment measured by CellTiter-Blue fluorescence assay (n=4 cultures). (**D**) Cell viability of 3D hiPSC-CMs 24 h post Cfz treatment using Live/Dead staining (red ethidium-stained cells were dead cells; green calcein-stained cells were live cells). Scale bar=100 μm. **(E)** Relative caspase3/7 activity of hiPSC-CMs 48 h post Cfz treatment (n=4-5 cultures). **(F)** Representative images of MitoSOX staining and summary of of MitoSOX MFI in hiPSC-CMs 24 and 48 h post Cfz treatment (n=3-4 cultures). Nuclei were counterstained with Hoechst. Scale bar=50 μm. (**G**) Relative cell viability of hiPSC-CMs 24 h following Cfz treatment with and without ascorbic acid (n=3 cultures). hiPSC-CMs were pre-treated with ascorbate acid for 2 h, followed by co-treatment with Cfz for 24 h. Cfz, carfilzomib; MFI, mean fluorescence intensity; D, day; h, hour.

**Figure 2**. **Cfz treatment reduced mitochondrial function of hiPSC-CMs.** (**A**) Measurement of TMRM fluorescence 24 h post Cfz treatment. Nuclei were counterstained with Hoechst. Scale bar=100 μm. (**B**) Summary of TMRM MFI analyzed by ArrayScan (n=5 cultures). (**C**) Effects of Cfz treatment on the expression of genes related to mitochondrial function in hiPSC-CMs (n=3 cultures). Gene expression is normalized to the housekeeping gene GAPDH and shown as relative levels to the control (DMSO-treated) group. (**D**) Representative traces of oxygen consumption rate recording in hiPSC-CMs upon sequential treatments with oligomycin, FCCP and a mixture of

rotenone and antimycin A. (**E**) Quantification of ATP production, basal respiration, and maximal respiration (n=4 cultures). The results were normalized to $1x10^6$ cells. (**F**) Relative cellular ATP content in 3D hiPSC-CMs 24 h post Cfz treatment as measured by an ATP-based luminescence assay (n=5 cultures). **, $P< 0.01$; ***, $P< 0.001$; ****, $P< 0.0001$. Cfz, carfilzomib; MFI, mean fluorescence intensity; OCR, oxygen consumption rate; h, hour; min, minute.

**Figure 3. Cfz increased abnormal intercellular $Ca^{2+}$ transients of hiPSC-CMs and decreased the expression of genes associated with $Ca^{2+}$ handling.** (**A**) Representative $Ca^{2+}$ transient traces from each group and summary of cells with normal and abnormal $Ca^{2+}$ transients (n=9-58 cells). hiPSC-CMs were treated with Cfz for 24 h and measured for $Ca^{2+}$ transients. Numbers shown on the stack bars represents percentages of cells with normal and abnormal $Ca^{2+}$ transients. (**B**) Relative expression levels of genes associated with $Ca^{2+}$ handling in hiPSC-CMs treated with Cfz for 24 h (n=3 cultures). *, $P<0.05$; ** $P<0.01$. Cfz, carfilzomib; h, hour; sec, second.

**Figure 4**. **Cfz treatment induced contractility dysfunction in 3D hiPSC-CMs.** (**A**) Pie chart representing proportions of spheroids with or without beating arrest 24 h post Cfz treatment (n=16-60 cardiac spheroids). (**B**) Contractility of static 3D hiPSC-CMs was video-recorded and analyzed using MATLAB. Representative heat maps and graphs of averaged magnitude of beating speed over time in Cfz-treated hiPSC-CMs. Red cycles and blue triangles represent contraction and relaxation, respectively. Note: hiPSC-CMs stopped beating following 24 h treatment of Cfz at 0.1, 1 and 10 μM. (**C**) Quantification of contraction, relaxation, and beating rate among groups (n=14-17 cardiac spheroids). (**D**) Expression of contractile proteins *MYH6* and *MYL2* detected by qRT-PCR (n=3 cultures). Cfz, carfilzomib; h, hour; sec, second.

**Figure 5. Cfz treatment reduced the traction forces of hiPSC-CMs.** For quantification of molecular traction forces of spontaneously contracting cardiomyocytes, hiPSC-CMs were treated for one day with Cfz and re-seeded on the glass bottom microplates coated with the DNA probes through biotin streptavidin conjugation. (**A**) Illustrative model of traction force measurement principle. The probes were decorated with peptide mimic (cRGDfk) of fibronectin, a fluorophore (Cy3B) and quencher (BHQ-2). Fluorescence intensity of the probes on the surface increases upon rupturing of the probes when cells contract and apply a force to the probes greater than the force tolerance of around 56 pN. (**B**) Summary of traction force measurement in hiPSC-CMs treated with Cfz *vs*. DMSO (n=20-30 cells). (**C**) Representative traction force microscopy of hiPSC-CMs post Cfz treatment. Scale bar=12 μm. Cfz, carfilzomib; RICM, reflection interference contrast microscopy; pN, pico newton.

**Figure 6. Cfz treatment led to structural alterations in hiPSC-CMs.** hiPSC-CMs were treated with Cfz for 24 h, fixed and stained with antibodies against α-actinin. Cell were imaged using fluorescence microscopy and quantitatively analyzed. (**A**) Representative RICM and fluorescence images of hiPSC-CMs treated with Cfz. Scale bar=12μm. (**B**) Summary of structural parameters of hiPSC-CMs post Cfz treatment (n=20-30 cells). Note that Cfz treatment significantly decreased the spread area, *z*-line length, and sarcomere length and increased circularity. Cells treated with Cfz at 1 and 10 μM did not show clear striation and z lines. Cfz, carfilzomib; RICM, reflection interference contrast microscopy; h, hour.

**Figure 7. Cfz treatment altered global gene expression in hiPSC-CMs.** Gene expression profiling of hiPSC-CMs post treatment with 1 μM Cfz for 24 h was analyzed by RNA-seq (n-=3 cultures). DEGs in cells post Cfz were compared to those in the cells treated with DMSO. Volcano plot representing 3114 downregulated genes and 1913 upregulated genes are depicted in the red and blue dots, respectively**.** DEGs between the 2 groups were defined based on adjusted *P* value < 0.05 and the absolute value of $\log_2$ (fold change) ≥ 1. (**B**) Bubble plots representing enrichment analysis of DEGs using GO enrichment analysis. **(C)** Chord diagram of relationship between selected GO terms and relevant DEGs. Each GO term is shown on the right, and genes contributing to these enrichments are presented on the left. Colored squares next to each gene indicate $\log_2$ (fold change) from the highest to the lowest level. (**D**) Heatmap of DEGs associated with cardiac muscle contraction (left) and ECM, integrin complex, and actinin cytoskeleton (right). Red color indicated relatively high expression and blue color indicated relatively low expression based on z-score. Cfz, carfilzomib; h, hour; GO, gene ontology; DEGs, differentially expressed genes.

**Figure 8. Profiling of proteins post Cfz treatment by proteomics.** DEPs were identified with abundance change by >1.3-fold [absolute $\log_2$(fold change) > 0.38] compared to the DMSO-treated group (n=3 cultures). (**A-B**) Volcano plot illustrating proteins in the cell lysate (right) and secreted proteins (left) with statistically significant abundance differences. Significantly upregulated proteins are marked in blue, and significantly downregulated proteins are in red. (**C-D**) Venn diagram showing overlapping of DEGs and DEPs post Cfz treatment in the cell lysate and the secretome. (**E**) Bubble plot represents selected GO terms based on overlapped DEGs and DEPs with significant upregulation. Cfz, carfilzomib; GO, gene ontology; DEGs, differentially expressed genes; DEPs, differentially expressed proteins.

**Figure 9. Profiling of protein changes in response to Cfz treatment in hiPSC-CMs.** (**A-B**) GO-term enrichment of the downregulated and upregulated proteins in the cell lysate. (**C**) GO-term enrichment of the downregulated secreted proteins**. (D)** Pearson correlation of biological triplicate experiments of control group (C1-3) and Cfz-treated group (T1-3). Pearson correlation coefficient (r) values are depicted for each group. Cfz, carfilzomib; GO, gene ontology.

**Table 1. Primers for quantitative reverse transcription polymerase chain reaction**

| Gene | Full name (another name) | Accession code | Primer |
|---|---|---|---|
| *ATP2A2* | ATPase, $Ca^{2+}$ transporting, cardiac muscle, slow twitch 2 | NM_170665 | Forward: TCAGCAGGAACTTTGTCACC Reverse: GGGCAAAGTGTATCGACAGG |
| *CASQ2* | Calsequestrin 2 | NM_001232 | Forward: TTATGTTCAAGGACCTGGGC Reverse: GCCTCTACTACCATGAGCCG |
| *GAPDH* | Glyceraldehyde-3-phosphate dehydrogenase | NM_001256799 | Forward: CTGGGCTACACTGAGCACC Reverse: AAGTGGTCGTTGAGGGCAATG |
| *MYH6* | Myosin, heavy chain 6, cardiac muscle, alpha (*α-MHC*) | NM_002471 | Forward: CTTCTCCACCTTAGCCCTGG Reverse: GCTGGCCCTTCAACTACAGA |
| *MYL2* | Myosin, light chain 2, regulatory, cardiac, slow (MLC-2V), | NM_000432 | Forward: CGTTCTTGTCAATGAAGCCA Reverse: CAACGTGTTCTCCATGTTCG |
| *RYR2* | Ryanodine receptor 2, cardiac | NM_001035 | Forward: CAAATCCTTCTGCTGCCAAG Reverse: CGAAGACGAGATCCAGTTCC |
| *SLC8A1* | Solute carrier family 8 (sodium/calcium exchanger), member 1 | NM_021097 | Forward: CTGGAATTCGAGCTCTCCAC Reverse: ACATCTGGAGCTCGAGGAAA |
| *OPA1* | OPA1 mitochondrial dynamin like GTPase | NM_015560.3 | Forward: TGAAAGCATCAAGTTTTTCTTG Reverse: TGCTGAAGATGGTGAGAAGAAG |
| *NDUFB5* | NADH ubiquinone oxoreductase subunit B5 | NM_002492.4 | Forward: ATGGTCTCCACTGTGTCGAA Reverse: GGTGGCAGCTCTGTCTGG |
| *MFN2* | Mitofusin 2 | NM_014874.4 | Forward: TTGCATCGAGAGAAGAGCAG Reverse: GTCTTTTGGACTTCAGCCAT |
| *MFN1* | Mitofusin 1 | NM_033540.3 | Forward: GTTTTCACTGCTGACTGCGA Reverse: GTGGCACTTGCTGAAGGATT |
| COQ10A | Coenzyme Q10 homolog A | NM_144576 | Forward: CTTACCTTCGAGCCGTTCCTT Reverse: CCATGATTCTACGCTCCGAGTA |

| | | | |
|---|---|---|---|
| UCP3 | Uncoupling Protein 3 | NM_003356.4 | Forward: AACGCAAAAAGGAGGGTGTA Reverse: CTCCAGGCCAGTACTTCAGC |

Note: primers were retrieved from open access websites (http://primerdepot.nci.nih.gov/ or http://pga.mgh.harvard.edu/primerbank/)

**Table 2. Top downregulated GO terms based on DEGs**

| GO term | Category | Number of Genes | Go term ID | *Adj P* value | Enrichment |
|---|---|---|---|---|---|
| Extracellular matrix | biological process | 106 | GO:0031012 | 1.24E-17 | 3.2 |
| Extracellular structure organization | cellular component | 108 | GO:0043062 | 2.02E-12 | 3 |
| Extracellular matrix structural constituent | morphological function | 54 | GO:0005201 | 1.37E-10 | 3.6 |
| Contractile fiber | biological process | 49 | GO:0043292 | 0.006207 | 2.3 |
| Transmembrane receptor protein serine/threonine kinase signaling pathway | cellular component | 68 | GO:0007178 | 0.007959 | 2.1 |
| Integrin complex | morphological function | 12 | GO:0008305 | 0.010804 | 3.4 |
| Actin binding | morphological function | 79 | GO:0003779 | 0.012514 | 2 |
| Integrin binding | biological process | 29 | GO:0005178 | 0.027535 | 2.5 |
| Pathway-restricted SMAD protein phosphorylation | biological process | 19 | GO:0060389 | 0.028713 | 3.1 |
| Cardiac muscle contraction | biological process | 31 | GO:0060048 | 0.028713 | 2.7 |
| Cardiac muscle tissue morphogenesis | biological process | 20 | GO:0055008 | 0.028713 | 3.2 |
| Response to calcium ion | biological process | 34 | GO:0051592 | 0.03831 | 2.4 |
| Muscle system process | biological process | 77 | GO:0003012 | 0.044283 | 1.8 |
| Sarcomere organization | cellular component | 14 | GO:0045214 | 0.046017 | 3.4 |
| Actin cytoskeleton | cellular component | 83 | GO:0015629 | 0.048669 | 1.7 |

GO, gene ontology; DEGs, differentially expressed genes.

**Table 3. Top 20 downregulated DEGs**

| Gene ID | Gene Symbol | Description | *Adj P* value | $Log_2$ (fold change) |
|---|---|---|---|---|
| ENSG00000177943 | *MAMDC4* | MAM domain containing 4 | 4.94E-56 | -9.199087572 |
| ENSG00000171992 | *SYNPO* | synaptopodin | 8.84E-51 | -6.60093912 |
| ENSG00000104738 | *MCM4* | minichromosome maintenance complex cor | 1.11E-50 | -6.261530975 |
| ENSG00000137809 | *ITGA11* | integrin subunit alpha 11 | 2.58E-48 | -6.196870403 |
| ENSG00000184347 | *SLIT3* | slit guance ligand 3 | 5.13E-46 | -6.157781163 |
| ENSG00000156427 | *FGF18* | fibroblast growth factor 18 | 6.14E-43 | -6.150872209 |
| ENSG00000185567 | *AHNAK2* | AHNAK nucleoprotein 2 | 3.69E-39 | -6.083552672 |
| ENSG00000128951 | *DUT* | deoxyurine triphosphatase | 7.18E-39 | -6.012024116 |
| ENSG00000225138 | *None* | None | 1.01E-38 | -5.979760829 |
| ENSG00000166482 | *MFAP4* | microfibril associated protein 4 | 2.35E-38 | -5.973236912 |
| ENSG00000107796 | *ACTA2* | actin alpha 2, smooth muscle | 4.87E-34 | -5.900336258 |
| ENSG00000162591 | *MEGF6* | multiple EGF like domains 6 | 5.24E-33 | -5.883525697 |
| ENSG00000179431 | *FJX1* | four-jointed box kinase 1 | 1.35E-31 | -5.691046545 |
| ENSG00000157637 | *SLC38A10* | solute carrier family 38 member 10 | 2.21E-31 | -5.669748257 |
| ENSG00000171130 | *ATP6V0E2* | ATPase H+ transporting V0 subunit e2 | 8.55E-31 | -5.627308177 |
| ENSG00000129103 | *SUMF2* | sulfatase modifying factor 2 | 9.96E-31 | -5.615074065 |
| ENSG00000100889 | *PCK2* | phosphoenolpyruvate carboxykinase 2, mitc | 1.01E-30 | -5.606701278 |
| ENSG00000228594 | *FNDC10* | fibronectin type III domain containing 10 | 1.94E-30 | -5.571960443 |
| ENSG00000091986 | *CCDC80* | coiled-coil domain containing 80 | 6.85E-30 | -5.561040949 |
| ENSG00000100297 | *MCM5* | minichromosome maintenance complex cor | 2.30E-29 | -5.547162364 |

DEGs, differentially expressed genes.

**Table 4. Top 20 upregulated DEGs**

| Gene ID | Gene Symbol | Description | *P* value | $Log_2$ (fold change) |
|---|---|---|---|---|
| ENSG00000198431 | *TXNRD1* | (thioredoxin reductase 1 | 4.82E-178 | 4.006453 |
| ENSG00000204388 | *HSPA1B* | heat shock protein family A (Hsp70) member 1B | 3.04E-168 | 6.043998 |
| ENSG00000173110 | *HSPA6* | heat shock protein family A (Hsp70) member 6 | 1.07E-140 | 10.52902 |
| ENSG00000178381 | *ZFAND2A* | zinc finger AN1-type containing 2A | 3.06E-140 | 4.963423 |
| ENSG00000080824 | *HSP90AA1* | heat shock protein 90 alpha family class A member 1 | 4.45E-120 | 3.567891 |
| ENSG00000204389 | *HSPA1A* | heat shock protein family H (Hsp110) member 1 | 1.35E-105 | 5.713138 |
| ENSG00000120694 | *HSPH1* | heat shock protein family H (Hsp110) member 1 | 4.87E-94 | 3.593188 |
| ENSG00000151929 | *BAG3* | BAG cochaperone 3 | 2.72E-90 | 3.825662 |
| ENSG00000187134 | *AKR1C1* | aldo-keto reductase family 1 member C1 | 7.03E-90 | 6.435566 |
| ENSG00000211445 | *GPX3* | glutathione peroxidase 3 | 2.76E-73 | 3.792141 |
| ENSG00000248713 | *C4orf54* | chromosome 4 open reading frame 54 | 7.41E-73 | 7.267963 |
| ENSG00000096384 | *HSP90AB1* | heat shock protein 90 alpha family class B member 1 | 1.18E-67 | 2.472503 |
| ENSG00000132002 | *DNAJB1* | DnaJ heat shock protein family (Hsp40) member B1 | 4.49E-66 | 4.255973 |
| ENSG00000013275 | *PSMC4* | proteasome 26S subunit, ATPase 4 | 3.71E-64 | 2.343216 |
| ENSG00000150991 | *UBC* | ubiquitin C | 1.83E-61 | 3.294192 |
| ENSG00000272899 | *ATP6V1FNB* | (ATP6V1F neighbor) | 6.66E-61 | 5.123917 |
| ENSG00000023909 | *GCLM* | glutamate-cysteine ligase modifier subunit) | 2.35E-60 | 3.747229 |
| ENSG00000116161 | *CACYBP* | calcyclin binding protein | 7.54E-56 | 2.419254 |
| ENSG00000197170 | *PSMD12* | proteasome 26S subunit, non-ATPase 12 | 1.96E-54 | 2.627123 |

DEGs, differentially expressed genes.

**Table 5. Top downregulated DEPs in cell lysate**

| Protein ID | Gene symbol | Description | *P* value | $Log_2$ (fold change) |
|---|---|---|---|---|
| P28161 | *GSTM2* | glutathione S-transferase mu 2 | 0.000199 | -0.37869 |
| Q5XKP0 | *QIL1*(*MICOS13*) | mitochondrial contact site and cristae organizing system subunit 13 | 0.000256 | -0.38072 |
| P14618 | *PKM* | pyruvate kinase M1/2 | 0.000615 | -0.3854 |
| O15067 | *PFAS* | phosphoribosylformylglycinamidine synthase | 0.001144 | -0.39249 |
| Q14254 | *FLOT2* | flotillin 2 | 0.001165 | -0.39616 |
| Q9H0R4 | *HDHD2* | haloacid dehalogenase like hydrolase domain containing 2) | 0.00178 | -0.39726 |
| P29218 | *IMPA1* | inositol monophosphatase 1 | 0.002187 | -0.39969 |
| P30041 | *PRDX6* | peroxiredoxin 6 | 0.002598 | -0.40337 |
| P08243 | *ASNS* | asparagine synthetase (glutamine-hydrolyzing | 0.003198 | -0.40509 |
| P60174 | *TPI1* | triosephosphate isomerase 1 | 0.003513 | -0.40568 |
| O43236 | *44078* | | 0.003934 | -0.40886 |
| Q3MHD2 | *LSM12* | LSM12 homolog | 0.004002 | -0.40938 |
| P48509 | *CD151* | CD151 molecule (Raph blood group | 0.004477 | -0.4101 |
| P15259 | *PGAM2* | phosphoglycerate mutase 2 | 0.005065 | -0.41576 |
| Q16836 | *HADH* | hydroxyacyl-CoA dehydrogenase) | 0.005345 | -0.41756 |
| Q99541 | *PLIN2* | (perilipin 2 | 0.006138 | -0.42144 |
| Q9Y235 | *APOBEC2* | apolipoprotein B mRNA editing enzyme catalytic subunit 2 | 0.006633 | -0.42492 |
| Q13813-2 | *SPTAN1* | spectrin alpha, non-erythrocytic 1 | 0.006885 | -0.43392 |
| O60669 | *SLC16A7* | solute carrier family 16 member 7 | 0.008852 | -0.43623 |
| Q96AX9 | *MIB2* | mindbomb E3 ubiquitin protein ligase 2 | 0.009051 | -0.44424 |
| P51553 | *IDH3G* | isocitrate dehydrogenase (NAD (+) 3 non-catalytic subunit gamma) | 0.009335 | -0.44433 |
| P08133 | *ANXA6* | annexin A6 | 0.009685 | -0.46695 |
| P17174 | *GOT1* | glutamic-oxaloacetic transaminase 1 | 0.011001 | -0.47138 |
| P10109 | *FDX1* | ferredoxin 1) | 0.014375 | -0.47543 |
| P43007 | *SLC1A4* | solute carrier family 1 member 4 | 0.014845 | -0.48642 |
| P30046 | *DDT* | D-dopachrome tautomerase | 0.017058 | -0.50283 |
| Q13315 | *ATM* | ATM serine/threonine kinase | 0.0171 | -0.50678 |
| P34949 | *MPI* | mannose phosphate isomerase | 0.018324 | -0.50884 |
| Q8IYM0 | *FAM186B* | family with sequence similarity 186 member B | 0.018496 | -0.51545 |
| Q9NX18 | *SDHAF2* | succinate dehydrogenase complex assembly factor 2 | 0.021519 | -0.51609 |
| P80723 | *BASP1* | brain abundant membrane attached signal protein 1 | 0.022129 | -0.52675 |
| O75223 | *GGCT* | gamma-glutamylcyclotransferase) | 0.022945 | -0.53503 |
| P17612 | *PRKACA* | protein kinase cAMP-activated catalytic subunit alpha | 0.02751 | -0.55372 |
| P00374 | *DHFR* | dihydrofolate reductas | 0.027565 | -0.5787 |
| Q8N111 | *CEND1* | cell cycle exits and neuronal differentiation 1 | 0.033353 | -0.61374 |
| B7Z596 | *TPM1* | tropomyosin 1 | 0.033428 | -0.72819 |

DEPs, differentially expressed proteins.

**Table 6. Top upregulated DEPs in cell lysate**

| Protein ID | Gene symbol | Description | *P* value | $Log_2$ (fold change) |
|---|---|---|---|---|
| *P17066* | *HSPA6* | heat shock protein family A (Hsp70) member 6) | *5.85E-06* | *2.920214* |
| Q8N6M9 | *ZFAND2A* | zinc finger AN1-type containing 2A | 8.86E-06 | 2.792291 |
| P18847 | *ATF3* | activating transcription factor 3) | 2.03E-05 | 2.655011 |
| Q15327 | *ANKRD1* | ankyrin repeat domain 1 | 2.93E-05 | 2.301373 |
| O76080 | *ZFAND5* | zinc finger AN1-type containing 5 | 5.43E-05 | 2.210395 |
| P08107 | *HSPA1A* | heat shock protein family A (Hsp70) member 1A | 6.26E-05 | 2.166783 |
| P38936 | *CDKN1A* | cyclin dependent kinase inhibitor 1 | 7.03E-05 | 2.135166 |
| Q9H0R8 | *GABARAPL1* | GABA type A receptor associated protein like 1 | 8.41E-05 | 1.985212 |
| P25685 | *DNAJB1* | DnaJ heat shock protein family (Hsp40) member B1 | 0.000163 | 1.945932 |
| P04035 | *HMGCR* | 3-hydroxy-3-methylglutaryl-CoA reductase | 0.000211 | 1.855423 |
| P61587 | *RND3* | Rho family GTPase 3 | 0.000249 | 1.649824 |
| Q01581 | *HMGCS1* | **3-**hydroxy-3-methylglutaryl-CoA synthase 1 | 0.000271 | 1.626212 |
| O15525 | *MAFG* | MAF bZIP transcription factor G | 0.000284 | 1.601714 |
| Q9H3F6 | *KCTD10* | potassium channel tetramerization domain containing 10 | 0.00037 | 1.507235 |
| Q9UDY4 | *DNAJB4* | DnaJ heat shock protein family (Hsp40) member B4 | 0.000379 | 1.484945 |
| P54868 | *HMGCS2* | 3-hydroxy-3-methylglutaryl-CoA synthase 2 | 0.000395 | 1.463084 |
| P02792 | *FTL* | ferritin light chain | 0.000444 | 1.432189 |
| Q9UBU8 | *MORF4L1* | mortality factor 4 like 1 | 0.000498 | 1.42401 |
| Q9BYN0 | *SRXN1* | sulfiredoxin 1 | 0.000514 | 1.416937 |
| Q92963 | *RIT1* | Ras like without CAAX 1 | 0.000551 | 1.341017 |
| P02511 | *CRYAB* | crystallin alpha B) | 0.000627 | 1.330892 |
| Q9UH92 | *MLX* | MAX dimerization protein MLX) | 0.000713 | 1.30305 |
| Q92598 | *HSPH1* | (heat shock protein family H (Hsp110) member 1) | 0.00072 | 1.288595 |
| Q99608 | *NDN* | necdin, MAGE family member | 0.000767 | 1.265368 |
| Q9BY42 | *RTFDC1* | replication termination factor 2 | 0.000826 | 1.221335 |
| Q13501 | *SQSTM1* | sequestosome 1 | 0.000845 | 1.207748 |
| P78362 | *SRPK2* | SRSF protein kinase 2 | 0.000887 | 1.198661 |
| Q9Y5A7 | *NUB1* | negative regulator of ubiquitin like proteins 1 | 0.000906 | 1.194131 |
| P68133 | *ACTA1* | actin alpha 1, skeletal muscle | 0.000913 | 1.178388 |
| O60333-3 | *KIF1B* | kinesin family member 1B | 0.000962 | 1.153891 |
| P62699 | *YPEL5* | yippee like 5 | 0.001058 | 1.125207 |
| O75794 | *CDC123* | cell division cycle 12 | 0.001082 | 1.097219 |
| O95817 | *BAG3* | BAG cochaperone 3 | 0.001229 | 1.091382 |
| O43164 | *PJA2* | praja ring finger ubiquitin ligase 2 | 0.001327 | 1.058091 |
| Q07352 | *ZFP36L1* | ZFP36 ring finger protein like 1 | 0.00139 | 1.046927 |
| O14950 | *MYL12B* | myosin light chain 12B | 0.001602 | 1.007005 |
| Q9UGL1 | *KDM5B* | lysine demethylase 5B | 0.001648 | 0.977882 |
| P24844 | *MYL9* | myosin light chain 9 | 0.001717 | 0.966276 |

| | | | | |
|---|---|---|---|---|
| Q9UK73 | *FEM1B* | fem-1 homolog B | 0.00174 | 0.953693 |
| Q8TEY7 | *USP33* | ubiquitin specific peptidase 33 | 0.001752 | 0.948084 |
| P0CG47 | *UBB* | ubiquitin B | 0.001801 | 0.928962 |
| P46976 | *GYG1* | glycogenin 1 | 0.001869 | 0.926016 |

DEPs, differentially expressed proteins.

**Table 7. Top dysregulated DEPs in secretome**

| Protein ID | Gene Symbol | Description | *P* value | $Log_2$ (fold change) |
|---|---|---|---|---|
| P01009 | *SERPINA1* | Serpin family A member 1 | 0.002177 | -1.01851 |
| P09871 | *C1S* | Complement C1s | 0.005218 | -0.71786 |
| Q9UBP4 | *DKK3* | Dickkop WNT signaling pathway inhibitor 3 | 0.00526 | 0.74339 |
| P08107 | *HSPA1A* | heat shock protein family A (Hsp70) member 1A | 0.005936 | 1.115906 |
| Q15063 | *POSTN* | periostin | 0.006501 | -0.55999 |
| O60814 | *HIST1H2BK* | H2B clustered | 0.006567 | -0.27213 |
| P55083 | *MFAP4* | microfibril associated protein 4 | 0.007602 | -0.69158 |
| Q86UP2 | *KTN1* | kinectin 1 | 0.011208 | 0.152319 |
| Q12841 | *FSTL1* | Follistatin like 1 | 0.012976 | -0.5254 |
| P08238 | *HSP90AB1* | heat shock protein 90 alpha family class B member 1 | 0.013136 | -0.13566 |
| P02461 | *COL3A1* | Collagen type III alpha 1 chain | 0.013179 | -0.55331 |
| P26038 | *MSN* | Moesin | 0.013885 | 0.42732 |
| O95373 | *IPO7* | importin 7 | 0.014671 | -0.63705 |
| P11142 | *HSPA8* | Heat shock protein family A (Hsp70) member 8 | 0.016105 | 0.364134 |
| P31946 | *YWHAB* | Tyrosine 3-monooxygenase/tryptophan 5-monooxygenase activation protein beta) | 0.016696 | 0.35428 |
| P08123 | *COL1A2* | Collagen type I alpha 2 chain | 0.017711 | -0.45736 |
| Q14315 | *FLNC* | Filamin C | 0.021456 | 0.693258 |
| P02751 | *FN1* | Fibronectin 1 | 0.021493 | -0.54779 |
| P13929 | *ENO3* | Enolase 3 | 0.024012 | -0.33332 |
| Q7Z7M1 | *GPR144* | ADGRD2 - adhesion G protein-coupled receptor D2 | 0.024362 | 3.30262 |
| P55072 | *VCP* | valosin containing protein | 0.025906 | 0.830314 |
| P05121 | *SERPINE1* | serpin family E member 1 | 0.027676 | 0.433167 |
| P26038 | *MSN* | moesin | 0.013885 | 0.42732 |
| P50502 | *ST13* | ST13 Hsp70 interacting protein | 0.044477 | 0.412665 |

DEPs, differentially expressed proteins.

**Table 8. Downregulated DEPs in secretome and their association with KEGG pathways**

| Gene ID | Gene Symbol | Description | *P* value | $Log_2$ (fold change) | KEGG Pathway |
|---|---|---|---|---|---|
| ENSG00000177943 | *MAMDC4* | MAM domain containing 4 | 4.94E-56 | -9.19909 | None |
| ENSG00000171992 | *SYNPO* | Synaptopodin | 8.84E-51 | -6.60094 | N/A |
| ENSG00000104738 | *MCM4* | Minichromosome maintenance complex component 4 | 1.11E-50 | -6.26153 | (ko04530) Tight junction; (hsa04530) Tight junction |
| ENSG00000137809 | *ITGA11* | Integrin subunit alpha 11 | 2.58E-48 | -6.19687 | (ko03030) DNA replication; (hsa03030) DNA replication; (ko04110) Cell cycle |
| ENSG00000184347 | *SLIT3* | Slit guidance ligand 3 | 5.13E-46 | -6.15778 | (ko05412) Arrhythmogenic right ventricular cardiomyopathy (ARVC); (hsa05412) Arrhythmogenic right ventricular cardiomyopathy; (ko04512) ECM-receptor interaction |
| ENSG00000156427 | *FGF18* | fibroblast growth factor 18 | 6.14E-43 | -6.15087 | (ko04360) Axon guidance; (hsa04360) Axon guidance |
| ENSG00000185567 | *AHNAK2* | AHNAK nucleoprotein 2 | 3.69E-39 | -6.08355 | (ko05218) Melanoma; (hsa05218) Melanoma; (ko05224) Breast cancer |
| ENSG00000128951 | *DUT* | Deoxyuridine triphosphatase | 7.18E-39 | -6.01202 | N/A |
| ENSG00000225138 | *SLC9A3-AS1* | None | 1.01E-38 | -5.97976 | (ko00240) Pyrimidine metabolism; (hsa00240) Pyrimidine metabolism; (hsanan01) drug metabolism |

DEPs, differentially expressed proteins; KEGG, Kyoto encyclopedia of genes and genomes.

**Table 9. GO terms and KEGG pathways associated with overlapped genes/proteins identified by DEPs from cell lysate and DEGs by RNA-seq.**

| Description | Category | Count | GO /KEGG term ID | adj *P* value | Enrichment |
|---|---|---|---|---|---|
| Response to heat | GO term biological processes | 15 | GO:0009408 | 1E-15 | 40 |
| Heat shock protein binding | GO term molecular functions | 10 | GO:0031072 | 7.9E-10 | 35 |
| ATPase regulator activity | GO term molecular functions | 6 | GO:0060590 | 5E-07 | 65 |
| ATPase activator activity | GO term molecular Functions | 4 | GO:0001671 | 0.00016 | 71 |
| Ferroptosis | KEGG pathway | 4 | ko04216 | 0.00079 | 44 |
| Necroptosis | KEGG pathway | 6 | hsa04217 | 0.00079 | 16 |
| Tau protein binding | GO term molecular functions | 4 | GO:0048156 | 0.001 | 39 |
| Myeloid cell activation involved in immune response | GO term biological processes | 9 | GO:0002275 | 0.00126 | 7.3 |
| Chaperone-mediated autophagy | GO term biological processes | 3 | GO:0061684 | 0.00158 | 83 |
| Positive regulation of ATPase activity | GO term biological processes | 4 | GO:0032781 | 0.002 | 32 |
| Apoptotic signaling pathway | GO term biological processes | 9 | GO:0097190 | 0.00251 | 6.5 |
| ATPase activity | GO term molecular functions | 7 | GO:0016887 | 0.00501 | 8.3 |
| Regulation of ATPase activity | GO term biological processes | 4 | GO:0043462 | 0.00631 | 22 |
| Cellular response to interleukin 1 | GO term biological processes | 5 | GO:0071347 | 0.01 | 12 |
| Interleukin-1-mediated signaling pathway | GO term biological processes | 4 | GO:0070498 | 0.01259 | 17 |
| Stress-activated MAPK cascade | GO term biological processes | 5 | GO:0051403 | 0.05012 | 7.7 |
| regulation of extrinsic apoptotic signaling pathway | GO term biological processes | 4 | GO:2001236 | 0.05012 | 11 |
| Intrinsic apoptotic signaling pathway pathway | GO term biological processes | 5 | GO:0097193 | 0.05012 | 7.7 |
| Regulation of intrinsic apoptotic signaling | GO term biological processes | 4 | GO:2001242 | 0.0631 | 11 |
| Response to oxidative stress | GO Biological Processes | 6 | GO:0006979 | 0.0631 | 5.8 |
| Extrinsic apoptotic signaling pathway via death domain receptors | GO term biological processes | 3 | GO:0008625 | 0.1 | 15 |
| Regulation of reactive oxygen species metabolic process | GO term biological processes | 4 | GO:2000377 | 0.1 | 8.9 |
| Autophagy | GO term biological processes | 6 | GO:0006914 | 0.11749 | 4.9 |
| Positive regulation of cell death | GO term biological processes | 7 | GO:0010942 | 0.12589 | 4.2 |
| Pathways in cancer | | 6 | hsa05200 | 0.15136 | 4.6 |

| | | | | | |
|---|---|---|---|---|---|
| | KEGG pathway | | | | |
| MAPK signaling pathway | KEGG pathway | 4 | ko04010 | 0.19953 | 7 |
| Apoptotic mitochondrial changes | GO term biological processes | 3 | GO:0008637 | 0.2138 | 11 |
| ATPase activity, coupled | GO term molecular functions | 4 | GO:0042623 | 0.2138 | 6.8 |
| macro autophagy | GO term biological processes | 4 | GO:0016236 | 0.35481 | 5.6 |
| cellular senescence | KEGG pathway | 3 | hsa04218 | 0.42658 | 7.7 |
| oxidoreductase activity | GO Molecular Functions | 6 | GO:0016491 | 0.43652 | 3.5 |
| PI3K-Akt signaling pathway | KEGG Pathway | 4 | ko04151 | 0.4466 | 5.2 |
| regulation of Ras protein signal transduction | GO term biological processes | 3 | GO:0046578 | 0.56234 | 6.8 |
| regulation of MAPK cascade | GO term biological processes | 5 | GO:0043408 | 0.025119 | 2.9 |
| Wnt signaling pathway | GO term biological processes | 4 | GO:0016055 | 0.031623 | 3.4 |
| cell-cell signaling by wnt | GO term biological processes | 4 | GO:0198738 | 0.031623 | 3.4 |
| ERK1 and ERK2 cascade | GO term biological processes | 3 | GO:0070371 | 0.039811 | 4 |
| regulation of MAP kinase activity | GO term biological processes | 3 | GO:0043405 | 0.039811 | 3.8 |

DEGs, differentially expressed genes; DEPs, differentially expressed proteins; GO, gene ontology; KEGG, Kyoto encyclopedia of genes and genomes; RNA-seq, RNA sequencing.

Figure 1

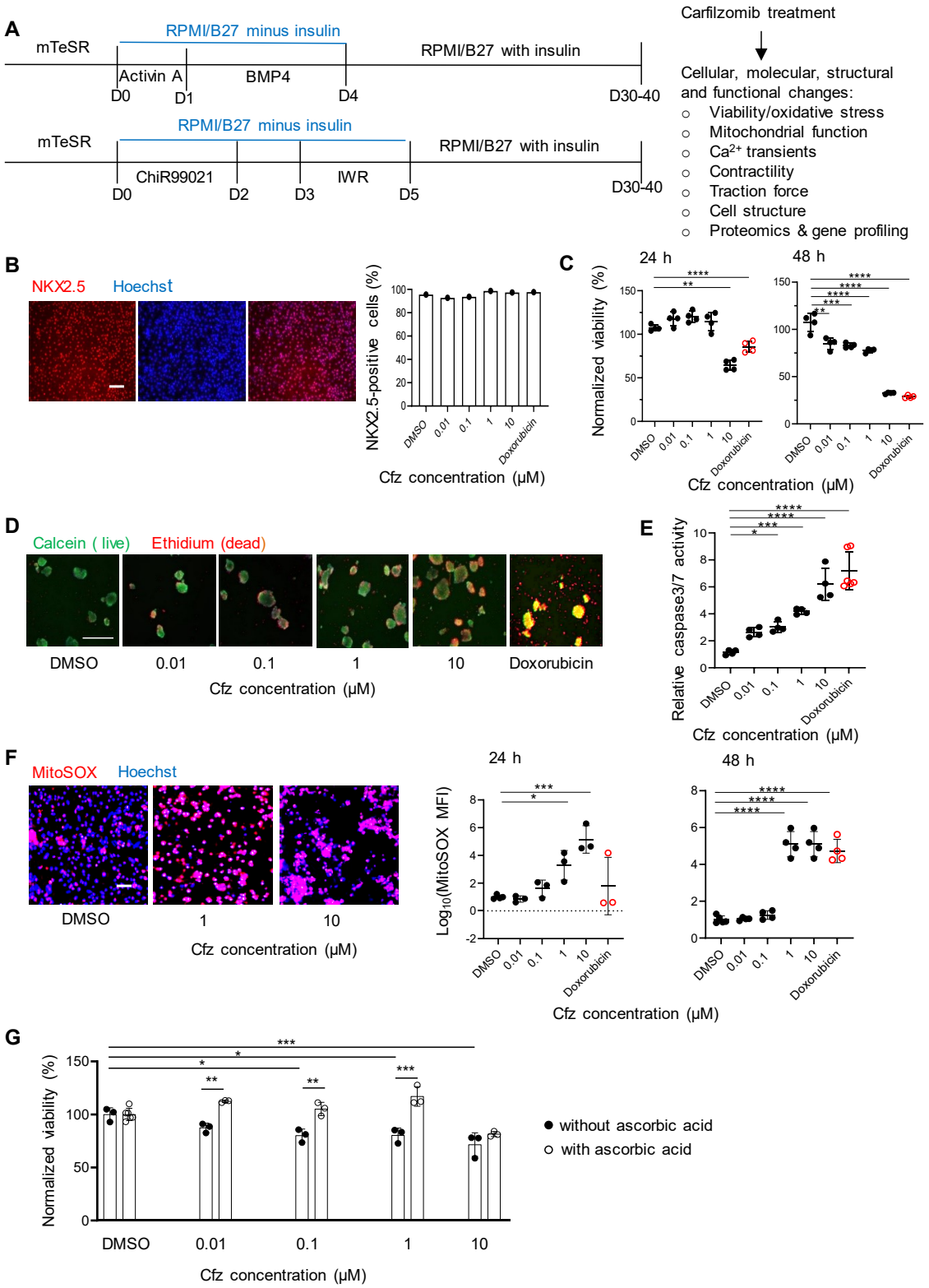
A
mTeSR
RPMI/B27 minus insulin
RPMI/B27 with insulin
Activin A
BMP4
D0
D1
D4
D30-40
mTeSR
RPMI/B27 minus insulin
RPMI/B27 with insulin
ChiR99021
IWR
D0
D2
D3
D5
D30-40
Carfilzomib treatment
Cellular, molecular, structural and functional changes:
Viability/oxidative stress
Mitochondrial function
Ca2+ transients
Contractility
Traction force
Cell structure
Proteomics & gene profiling
B
NKX2.5
Hoechst
NKX2.5-positive cells (%)
DMSO
0.01
0.1
1
10
Doxorubicin
Cfz concentration (μM)
C
24 h
48 h
Normalized viability (%)
Cfz concentration (μM)
D
Calcein ( live)
Ethidium (dead)
DMSO
0.01
0.1
1
10
Doxorubicin
Cfz concentration (μM)
E
Relative caspase3/7 activity
Cfz concentration (μM)
F
MitoSOX
Hoechst
DMSO
1
10
Cfz concentration (μM)
24 h
48 h
Log10(MitoSOX MFI)
Cfz concentration (μM)
G
Normalized viability (%)
DMSO
0.01
0.1
1
10
Cfz concentration (μM)
without ascorbic acid
with ascorbic acid

Figure 2

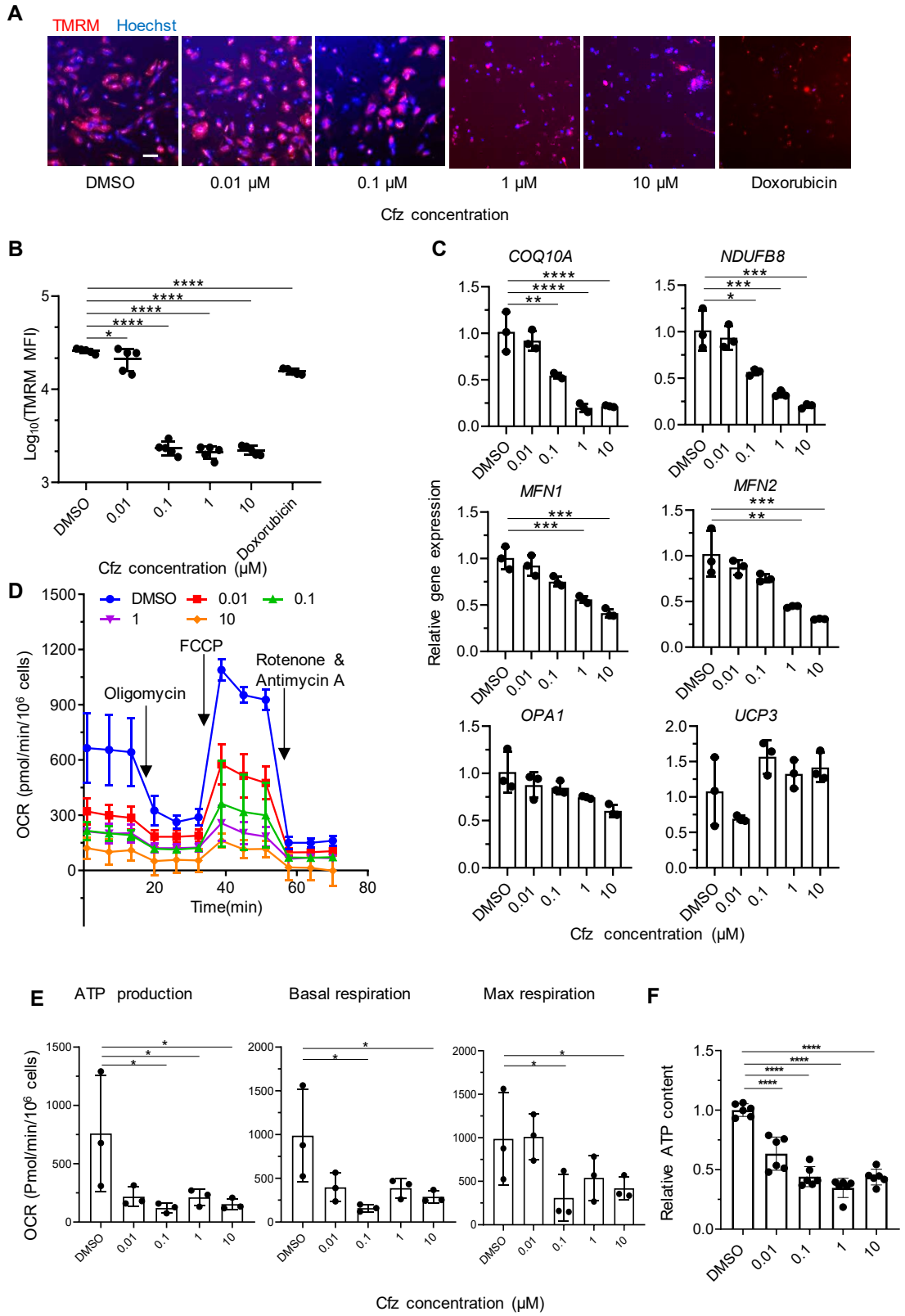
A
TMRM Hoechst
DMSO
0.01 μM
0.1 μM
1 μM
10 μM
Doxorubicin
Cfz concentration
B
Log10(TMRM MFI)
Cfz concentration (μM)
C
COQ10A
NDUFB8
MFN1
MFN2
OPA1
UCP3
Relative gene expression
Cfz concentration (μM)
D
DMSO
0.01
0.1
1
10
FCCP
Rotenone & Antimycin A
Oligomycin
OCR (pmol/min/10^6 cells)
Time(min)
E
ATP production
Basal respiration
Max respiration
OCR (Pmol/min/10^6 cells)
Cfz concentration (μM)
F
Relative ATP content

Figure 3

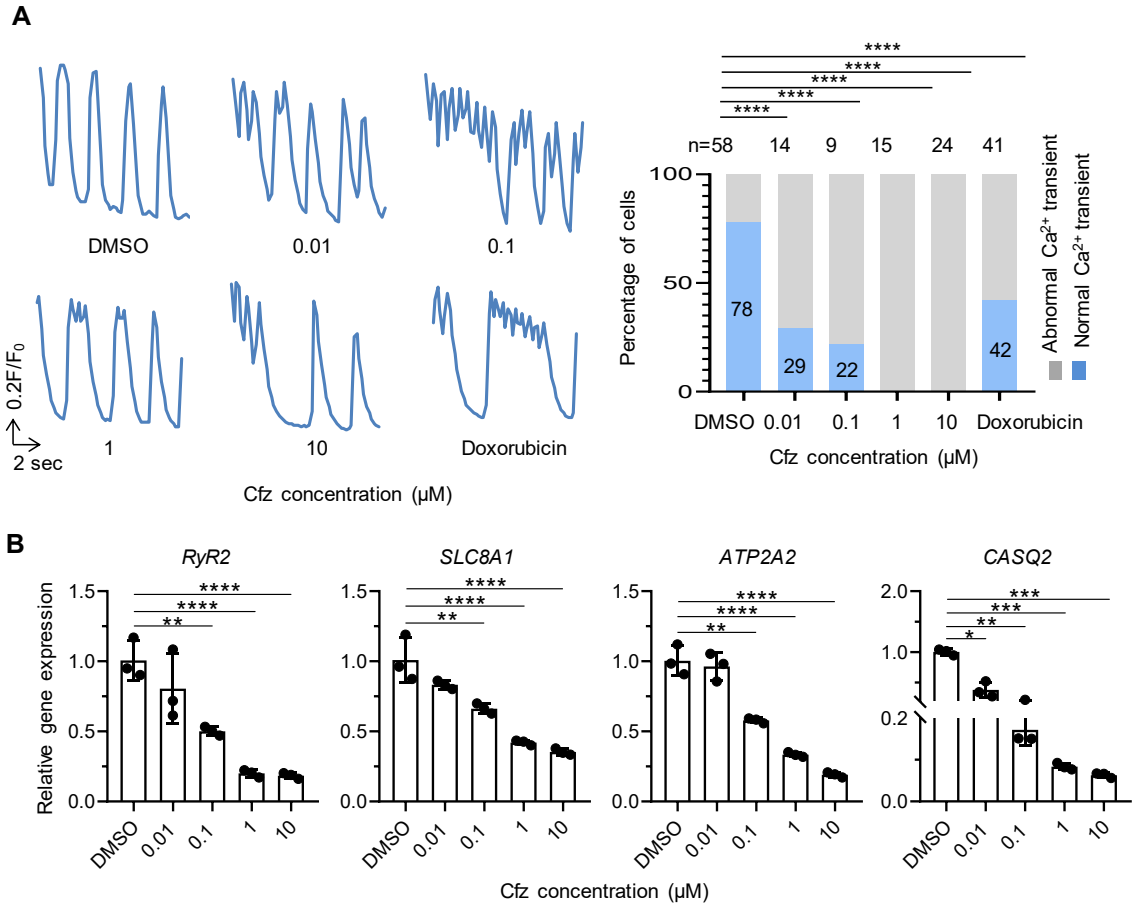
A
DMSO
0.01
0.1
1
10
Doxorubicin
0.2F/F0
2 sec
Cfz concentration (μM)
n=58 14 9 15 24 41
Percentage of cells
78
29
22
42
Abnormal Ca2+ transient
Normal Ca2+ transient
DMSO 0.01 0.1 1 10 Doxorubicin
Cfz concentration (μM)
B
RyR2
SLC8A1
ATP2A2
CASQ2
Relative gene expression
Cfz concentration (μM)

Figure 4

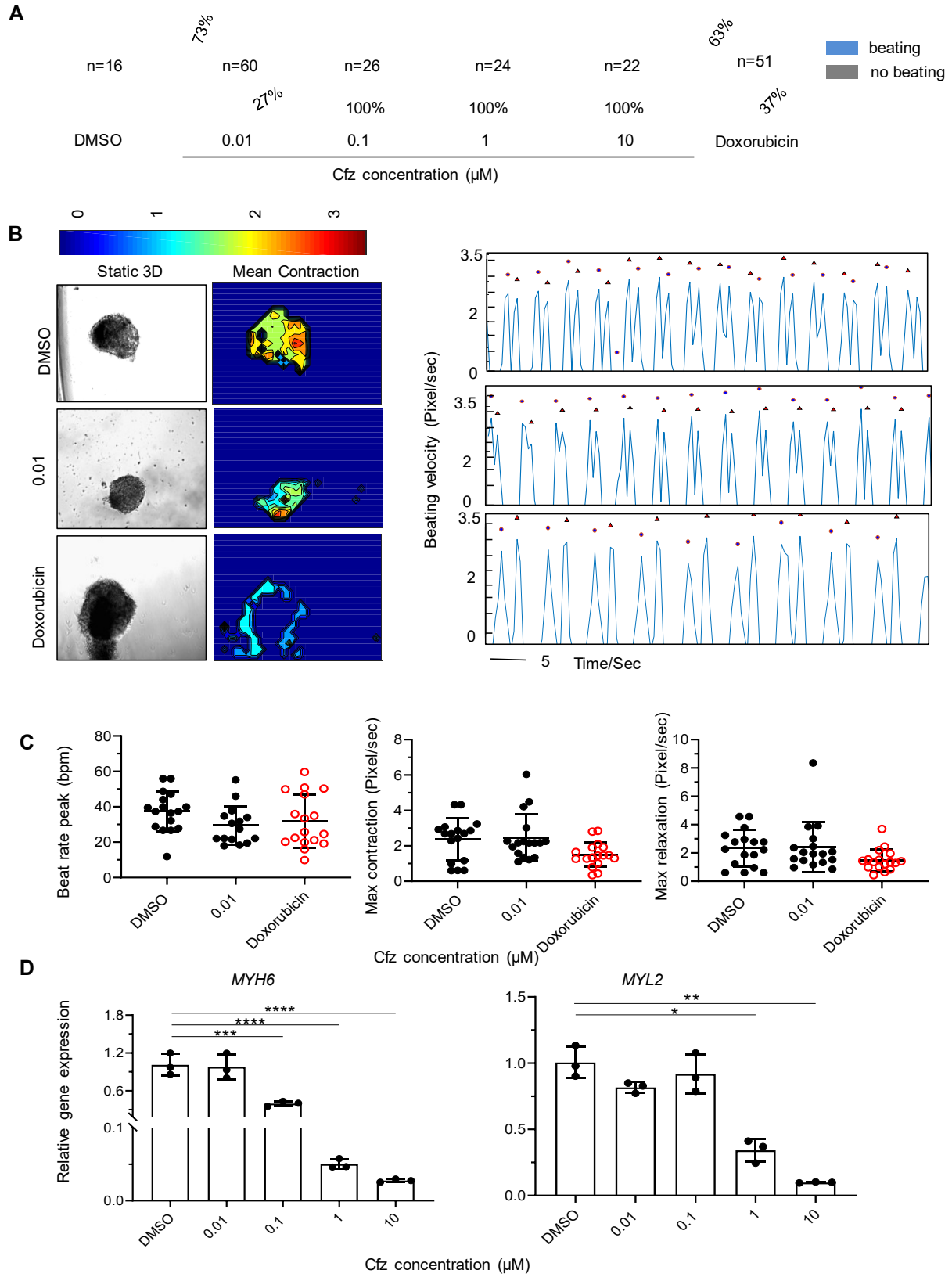
A
73%
63%
n=16
n=60
n=26
n=24
n=22
n=51
beating
no beating
27%
100%
100%
100%
37%
DMSO
0.01
0.1
1
10
Doxorubicin
Cfz concentration (μM)
B
0
1
2
3
Static 3D
Mean Contraction
DMSO
0.01
Doxorubicin
Beating velocity (Pixel/sec)
3.5
2
0
5
Time/Sec
C
Beat rate peak (bpm)
80
60
40
20
0
Max contraction (Pixel/sec)
8
6
4
2
0
Max relaxation (Pixel/sec)
10
8
6
4
2
0
DMSO
0.01
Doxorubicin
Cfz concentration (μM)
D
MYH6
MYL2
Relative gene expression
****
****
***
**
*
1.8
1.2
0.6
0.1
0.0
1.5
1.0
0.5
0.0
DMSO
0.01
0.1
1
10
Cfz concentration (μM)

Figure 5

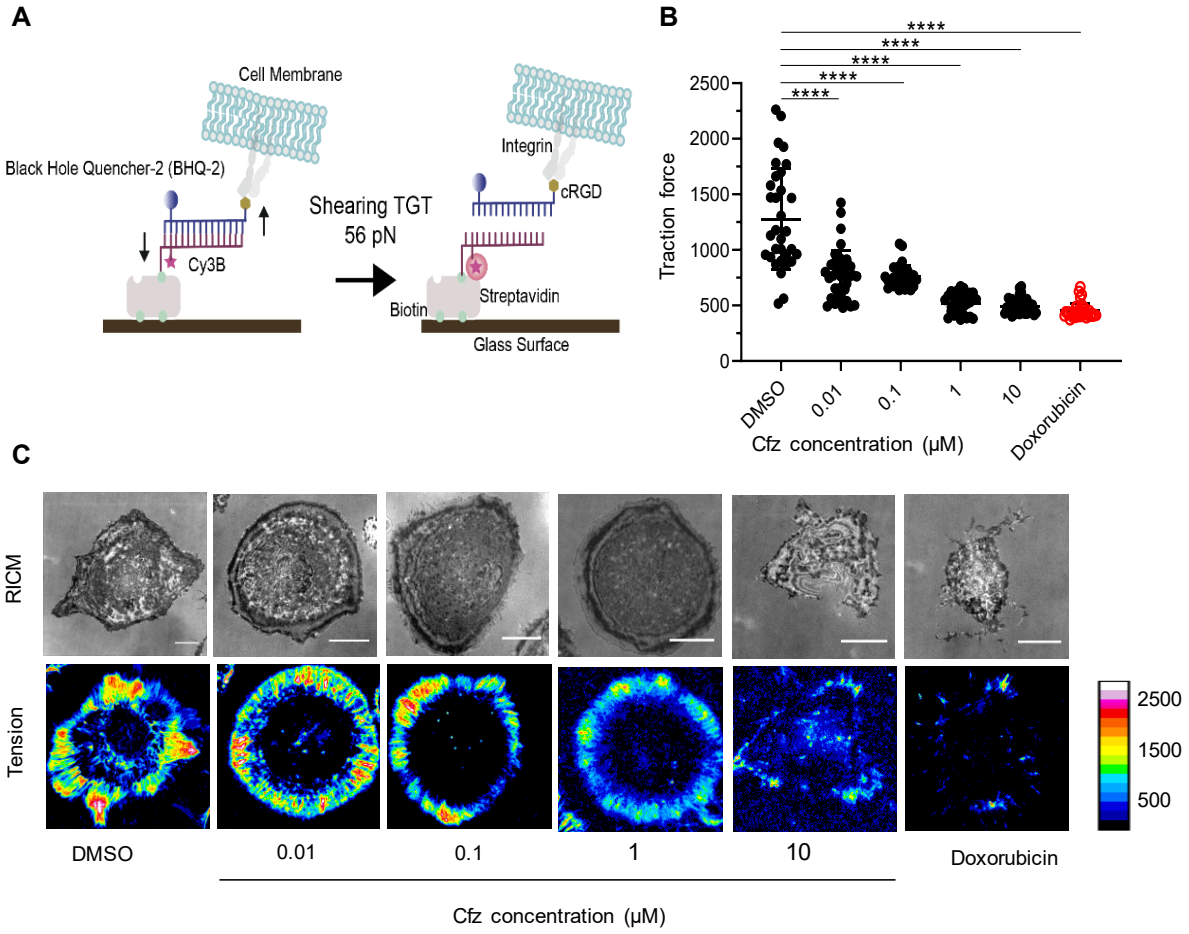
A
Cell Membrane
Black Hole Quencher-2 (BHQ-2)
Cy3B
Shearing TGT
56 pN
Integrin
cRGD
Streptavidin
Biotin
Glass Surface
B
Traction force
2500
2000
1500
1000
500
0
****
****
****
****
****
DMSO
0.01
0.1
1
10
Doxorubicin
Cfz concentration (μM)
C
RICM
Tension
2500
1500
500
DMSO
0.01
0.1
1
10
Doxorubicin
Cfz concentration (μM)

Figure 6

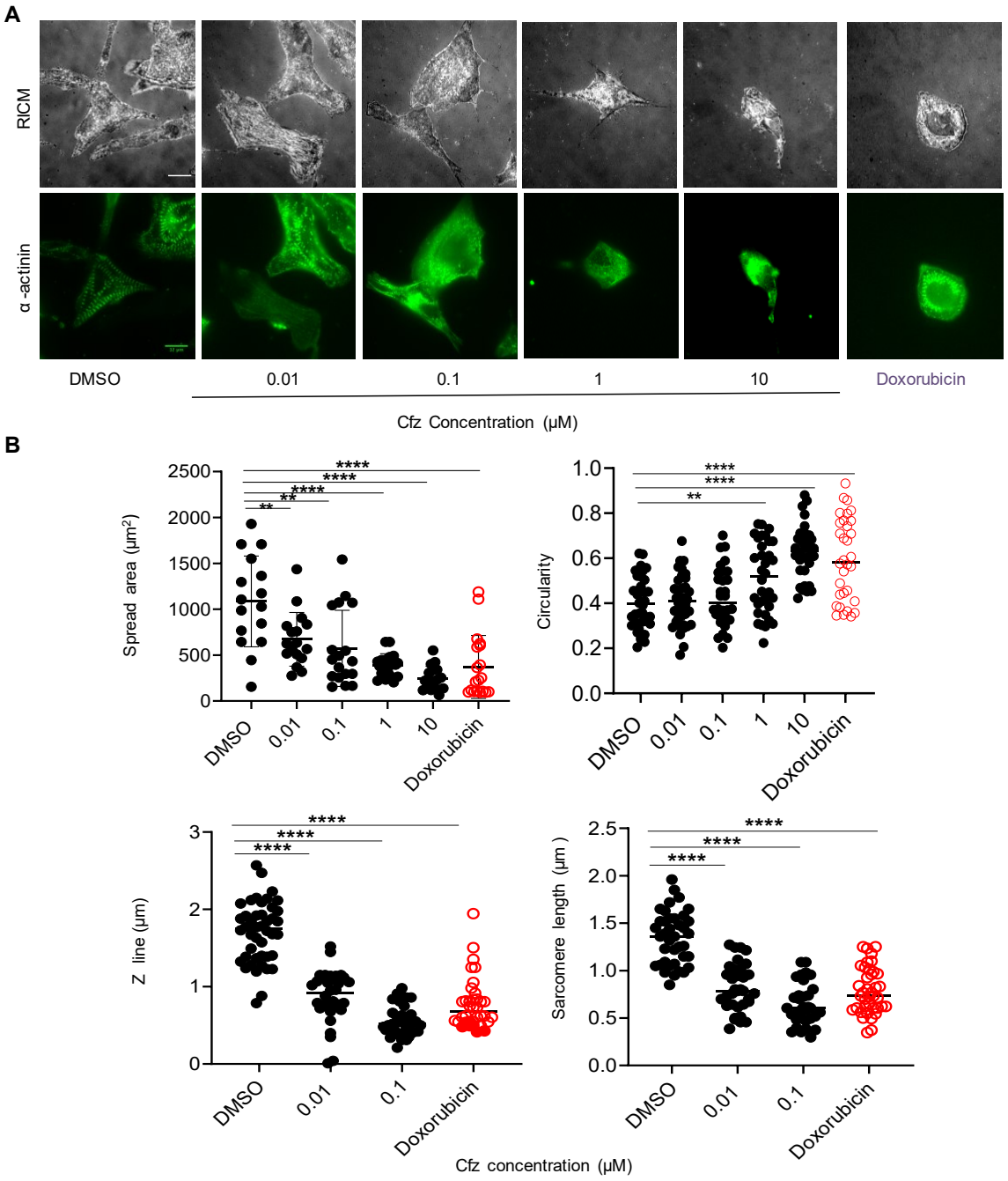
A
RICM
α -actinin
DMSO
0.01
0.1
1
10
Doxorubicin
Cfz Concentration (μM)
B
Spread area (μm²)
Circularity
Z line (μm)
Sarcomere length (μm)
Cfz concentration (μM)

Figrue 7

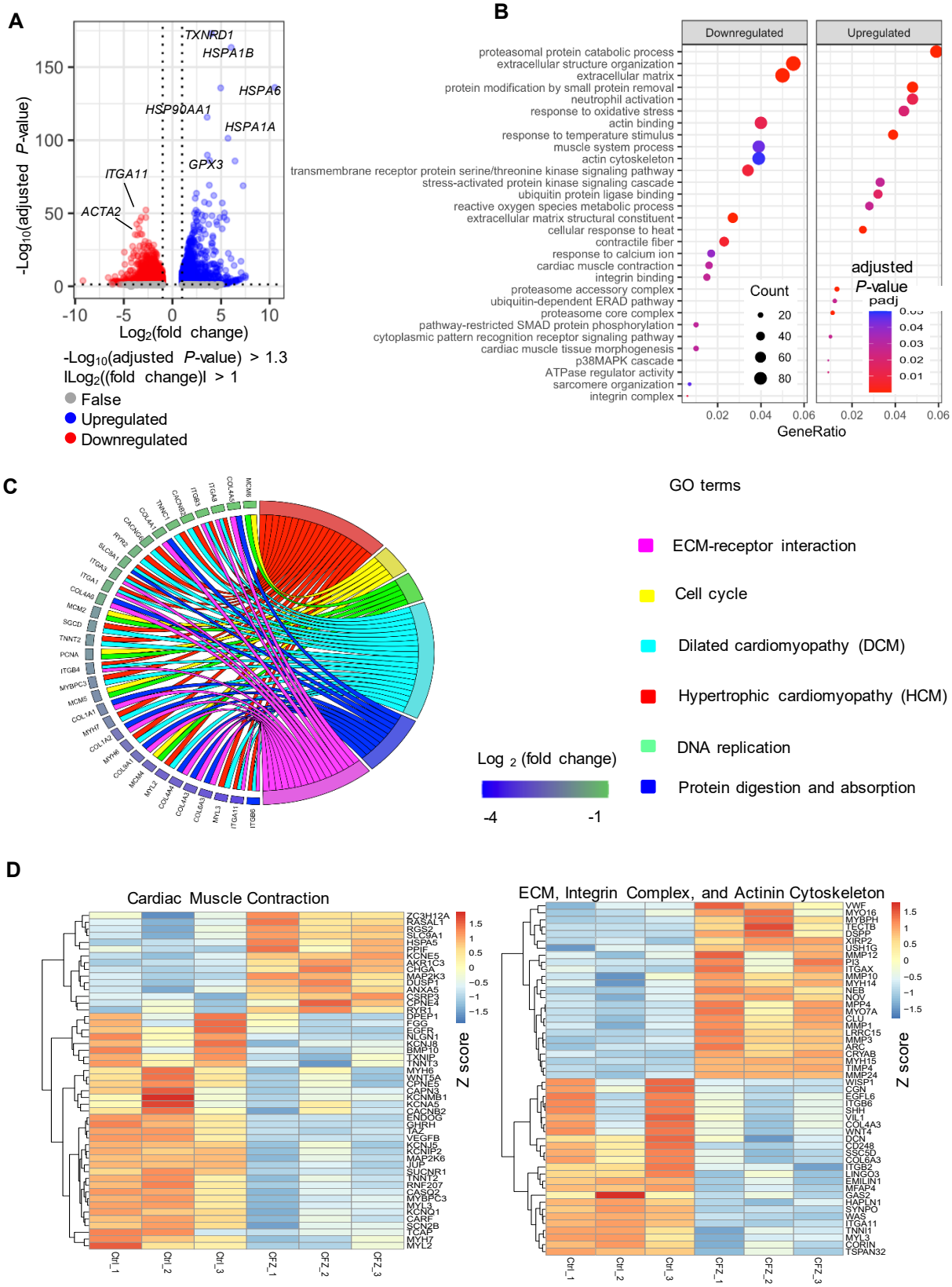
A
TXNRD1
HSPA1B
HSPA6
HSP90AA1
HSPA1A
GPX3
ITGA11
ACTA2
-Log10(adjusted P-value)
Log2(fold change)
-Log10(adjusted P-value) > 1.3
|Log2((fold change)| > 1
False
Upregulated
Downregulated
B
Downregulated
Upregulated
proteasomal protein catabolic process
extracellular structure organization
extracellular matrix
protein modification by small protein removal
neutrophil activation
response to oxidative stress
actin binding
response to temperature stimulus
muscle system process
actin cytoskeleton
transmembrane receptor protein serine/threonine kinase signaling pathway
stress-activated protein kinase signaling cascade
ubiquitin protein ligase binding
reactive oxygen species metabolic process
extracellular matrix structural constituent
cellular response to heat
contractile fiber
response to calcium ion
cardiac muscle contraction
integrin binding
proteasome accessory complex
ubiquitin-dependent ERAD pathway
proteasome core complex
pathway-restricted SMAD protein phosphorylation
cytoplasmic pattern recognition receptor signaling pathway
cardiac muscle tissue morphogenesis
p38MAPK cascade
ATPase regulator activity
sarcomere organization
integrin complex
Count
adjusted P-value
padj
GeneRatio
C
GO terms
ECM-receptor interaction
Cell cycle
Dilated cardiomyopathy (DCM)
Hypertrophic cardiomyopathy (HCM)
DNA replication
Protein digestion and absorption
Log 2 (fold change)
D
Cardiac Muscle Contraction
ECM, Integrin Complex, and Actinin Cytoskeleton
Z score
Ctrl_1
Ctrl_2
Ctrl_3
CFZ_1
CFZ_2
CFZ_3

Figrue 8

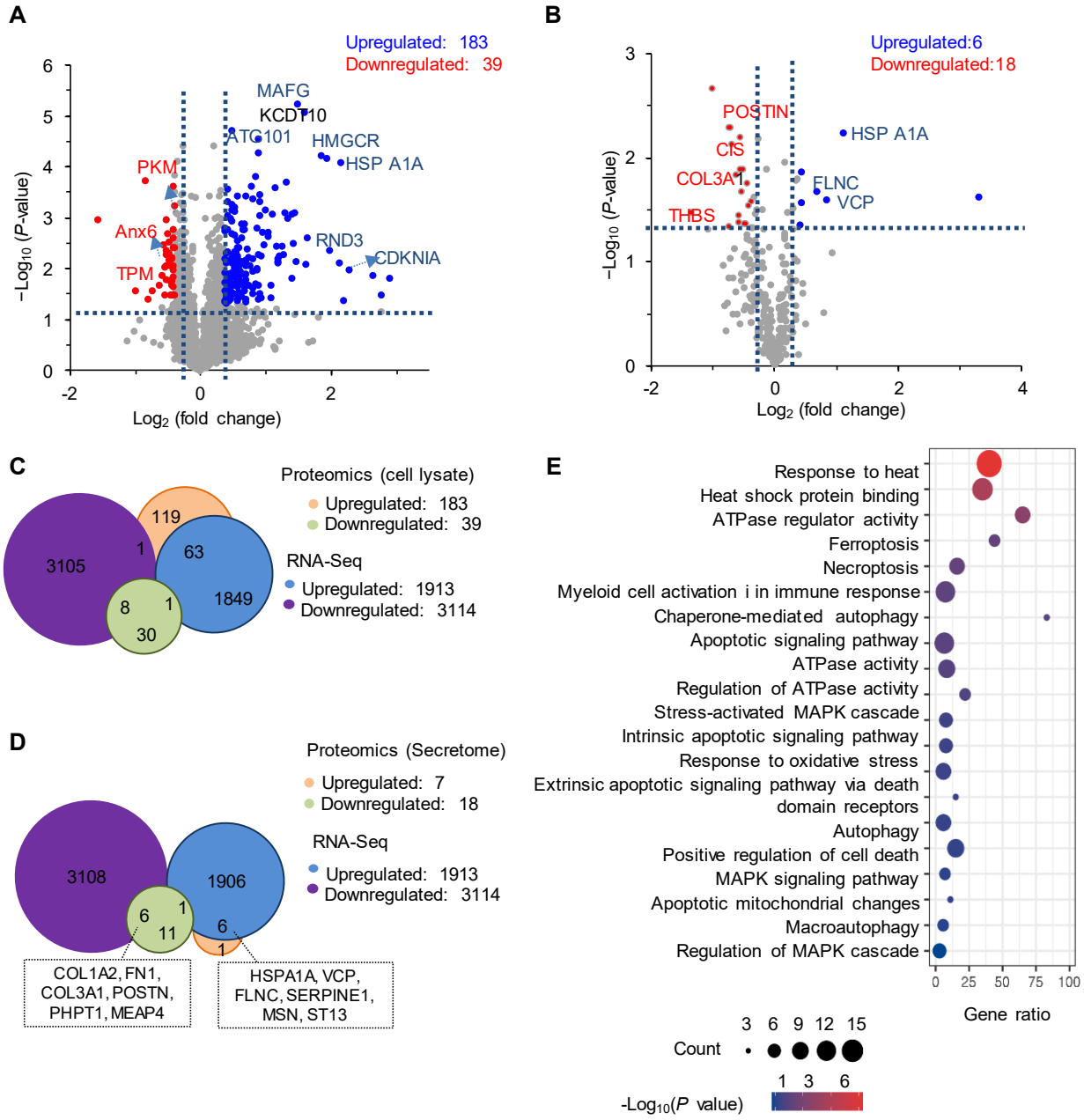
A
Upregulated: 183
Downregulated: 39
MAFG
KCDT10
ATG101
HMGCR
HSP A1A
PKM
Anx6
RND3
CDKNIA
TPM
−Log10 (P-value)
Log2 (fold change)
B
Upregulated:6
Downregulated:18
POSTN
CIS
COL3A1
THBS
HSP A1A
FLNC
VCP
−Log10 (P-value)
Log2 (fold change)
C
Proteomics (cell lysate)
Upregulated: 183
Downregulated: 39
RNA-Seq
Upregulated: 1913
Downregulated: 3114
3105
119
1
63
1849
8
1
30
D
Proteomics (Secretome)
Upregulated: 7
Downregulated: 18
RNA-Seq
Upregulated: 1913
Downregulated: 3114
3108
1906
6
1
11
6
1
COL1A2, FN1, COL3A1, POSTN, PHPT1, MEAP4
HSPA1A, VCP, FLNC, SERPINE1, MSN, ST13
E
Response to heat
Heat shock protein binding
ATPase regulator activity
Ferroptosis
Necroptosis
Myeloid cell activation i in immune response
Chaperone-mediated autophagy
Apoptotic signaling pathway
ATPase activity
Regulation of ATPase activity
Stress-activated MAPK cascade
Intrinsic apoptotic signaling pathway
Response to oxidative stress
Extrinsic apoptotic signaling pathway via death domain receptors
Autophagy
Positive regulation of cell death
MAPK signaling pathway
Apoptotic mitochondrial changes
Macroautophagy
Regulation of MAPK cascade
Gene ratio
Count
-Log10(P value)

Figrue 9

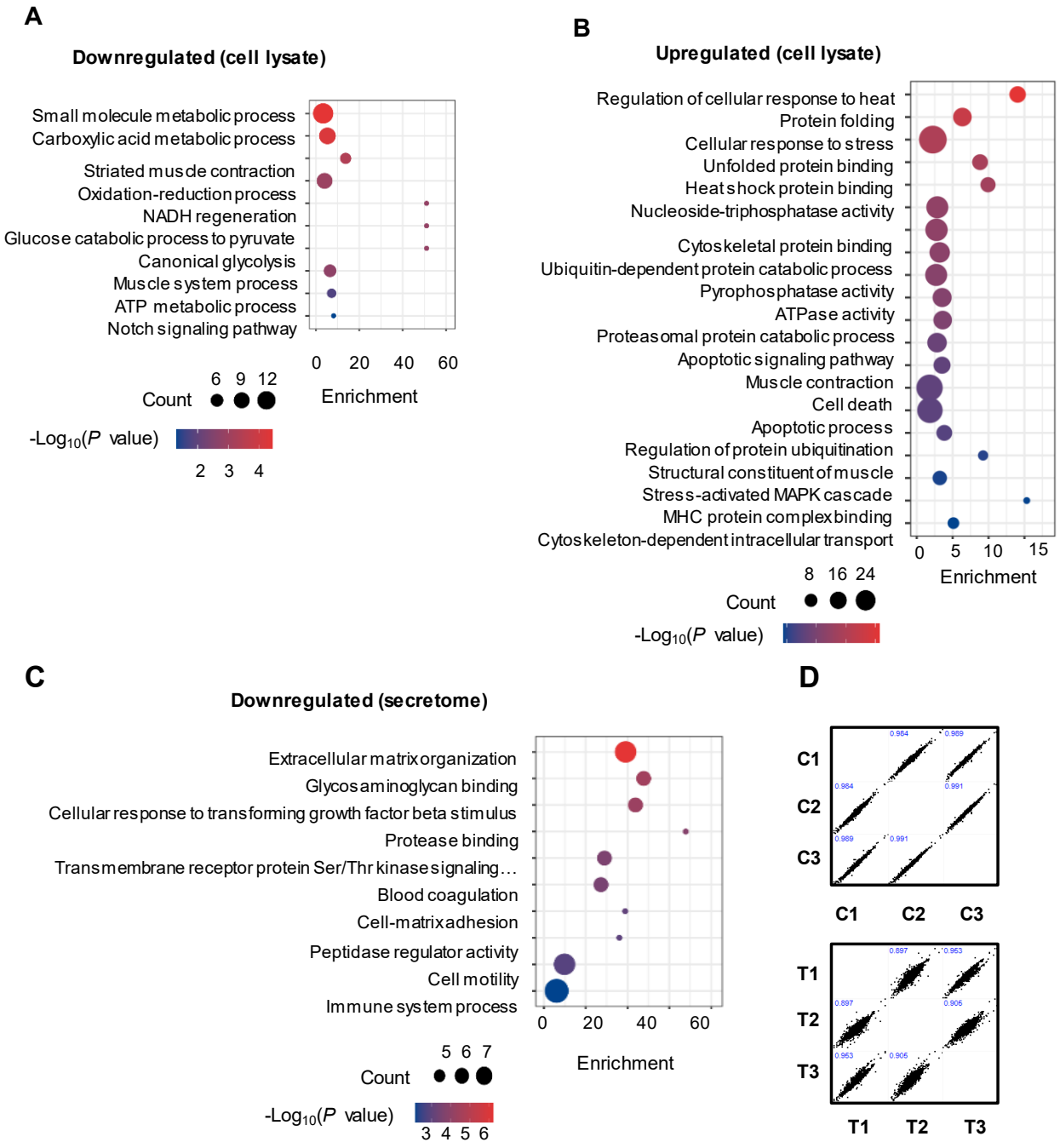
A
Downregulated (cell lysate)
Small molecule metabolic process
Carboxylic acid metabolic process
Striated muscle contraction
Oxidation-reduction process
NADH regeneration
Glucose catabolic process to pyruvate
Canonical glycolysis
Muscle system process
ATP metabolic process
Notch signaling pathway
0 20 40 60
Enrichment
6 9 12
Count
-Log10(P value)
2 3 4
B
Upregulated (cell lysate)
Regulation of cellular response to heat
Protein folding
Cellular response to stress
Unfolded protein binding
Heat shock protein binding
Nucleoside-triphosphatase activity
Cytoskeletal protein binding
Ubiquitin-dependent protein catabolic process
Pyrophosphatase activity
ATPase activity
Proteasomal protein catabolic process
Apoptotic signaling pathway
Muscle contraction
Cell death
Apoptotic process
Regulation of protein ubiquitination
Structural constituent of muscle
Stress-activated MAPK cascade
MHC protein complex binding
Cytoskeleton-dependent intracellular transport
0 5 10 15
Enrichment
8 16 24
Count
-Log10(P value)
C
Downregulated (secretome)
Extracellular matrix organization
Glycosaminoglycan binding
Cellular response to transforming growth factor beta stimulus
Protease binding
Transmembrane receptor protein Ser/Thr kinase signaling…
Blood coagulation
Cell-matrix adhesion
Peptidase regulator activity
Cell motility
Immune system process
0 20 40 60
Enrichment
5 6 7
Count
-Log10(P value)
3 4 5 6
D
C1
C2
C3
0.964
0.989
0.964
0.991
0.989
0.991
C1 C2 C3
T1
T2
T3
0.897
0.963
0.897
0.905
0.963
0.905
T1 T2 T3